Tutorial Handout of ASME Turbo Expo 2024
Turbomachinery Technical Conference and Exposition
GT2024-TOB047
June 24-28, 2024

KNOW HOW ON

SQUEEZE FILM DAMPERS FOR AIRCRAFT ENGINES

ENGINEERING MODELS & EXPERIMENTAL VERIFICATION

Luis San Andrés
Professor Emeritus
Texas A&M University, College Station, TX 77845, USA
Lsanandres@tamu.edu http://rotorlab.tamu.edu

TUTORIAL DESCRIPTION

Squeeze Film Dampers (SFDs) are effective means to ameliorate rotor vibration amplitudes and to suppress instabilities in rotor-bearing systems. A SFD is not an off-the-shelf mechanical element but tailored to a particular rotor-bearing system as its design must satisfy a desired damping ratio; if too low, the damper is ineffective, whereas if damping is too large, the SFD may lock thus aggravating the system response. In many cases, SFDs are also employed to control the placement of (rigid body) critical speeds displacing the machine operation into a speed range ensuring an effective structural isolation.

Industry demands well-engineered SFDs with a low footprint to reduce cost, maintenance, weight, and space while pushing for higher operating shaft speeds to increase power output. Modern air breathing gas turbine engines implement ultra-short length SFDs ($L/D \leq 0.2$) to satisfy stringent weight and space demands with low parts count. Despite the myriad of analyses and experimental results reported in the literature, there is not a concerted effort to investigate the dynamic forced performance of a SFD through its many configurations: open ends vis-à-vis sealed ends conditions (Orings and piston rings), and supply conditions with a fluid plenum or deep groove vis-à-vis feed holes directly impinging into the film land. The tutorial reviews SFD experimental results and model prediction validations for damping and inertia force coefficients of several SFD configurations operating over a wide range of conditions.

OUTCOMES or LEARNING OBJECTIVES

The tutorial[1] reviews how SFDs generate viscous dissipation forces and fluid inertia forces aiding to reduce rotor vibrations. The knowledge extends to describe modern predictive tools vis a vis test data, a discussion on pervasive air ingestion at high whirl frequencies, and an effective selection of end seals to increase the available damping. Pressing questions on the design and operation of SFDs are answered.

The bulk of the tutorial presents comparisons of experimentally identified damping (C) and inertia or added mass (M) coefficients versus amplitude of motion (orbit size) and static eccentricity position, both ranging from small to large amplitudes The experimental results answer practical questions:

(a) How come SFDs do not have a stiffness (static centering ability)?

(b) Are SFDs just journal bearings that do not spin?

(c) Why do SFDs show a significant added or virtual mass?

(d) How much more damping is available if the damper has end seals?
Are piston rings better than O-rings? Which type to choose?

(e) Is a damper with feed holes as effective as one containing a central groove?
What if a hole plugs, is a damper still effective?

(f) Do the amplitude and shape of whirl motion affect the SFD force coefficients?

[1] This document updates knowledge in [1] San Andrés, L., 2010, *Modern Lubrication Theory*, "Squeeze Film Dampers," Notes 13, Texas A&M University Digital Libraries, http://oaktrust.library.tamu.edu/handle/1969.1/93197

(g) Is air ingestion a persistent issue with SFDs, open ends or sealed ends? Tell me how to quantify the amount of gas ingested in actual operation.

(h) How do predictions from classical and modern SFD models correlate with the experimental record?

(i) How do Integral SFDs work? Are ISFDs used in industry?

The tutorial sums the outcome of 30+ years of SFD experimental research, computational physics modeling, and engineering design conducted by the presenter and graduate students at the Turbomachinery Laboratory of Texas A&M University.

Background [1]

Squeeze film bearing dampers are lubricated elements providing viscous damping in mechanical systems. Squeeze film dampers in rotating machinery provide structural isolation, reduce the amplitudes of rotor response to imbalance, and in some instances, assist to suppress rotordynamic instability.

The most commonly recurring problems in rotordynamics are excessive steady state synchronous vibration levels and subsynchronous rotor instabilities. The first problem may be reduced by improved balancing, or by introducing modifications into the rotor-bearing system to move the system critical speeds out of the operating range, or by introducing external damping to limit peak amplitudes at traversed critical speeds. Subsynchronous rotor instabilities may be avoided by eliminating the instability mechanism, by rising the natural frequency of the rotor-bearing system as high as possible, or by introducing damping to increase the onset rotor speed of instability [2,3].

Lightweight, high-performance engines exhibit a trend towards increased flexibility leading to a high sensitivity to imbalance with large vibration levels and reduced reliability. Squeeze film dampers (SFDs) are essential components of high-speed turbomachinery since they offer the unique advantages of dissipation of vibration energy and isolation of structural components, as well as the capability to improve the dynamic stability characteristics of inherently unstable rotor-bearing systems. SFDs are used primarily in aircraft jet engines to provide viscous damping to rolling element bearings which themselves have little or no damping. One other important application is related to high performance compressor units where SFDs are installed in series with tilting pad bearings to reduce (soften) bearing support stiffness while providing additional damping as a safety mechanism to prevent rotordynamic instabilities. In addition, in geared compressors, the SFD assists to reduce and isolate multiple frequency excitations transmitted through the bull gear, for example.

Zeidan et al. [4] (1996) provide a history of the SFD in jet engines and detail design practices for successful SFD operation in commercial oil and gas centrifugal compressors. Adilleta and Della Pietra [5] in 2002 present a comprehensive review of the analytical and experimental work conducted on SFDs until 2000. Later in 2016, San Andrés et al. [6,7] discuss significant advances on SFD experiments, identification of force coefficients, and physical models for aircraft engines applications.

Despite the many successful applications, industry often recognizes that the design of SFDs is based on overly simplified predictive models that either fail to incorporate or simply neglect unique features (structural and fluidic) that affect the damper dynamic force performance. Actual damper performance can range from erratic to non-functioning depending on the operating conditions. Issues such as the fluid inertia, the influence of deep deed grooves, and lubricant cavitation vs. air entrainment are of continued interest, as detailed by San Andrés et al. in Refs. [8] (2003), [9] (2010), [10] (2020) and [11] (2023).

Fundamentals of the application

Figure 1 shows a typical SFD configuration consisting of an inner nonrotating journal and a stationary outer bearing, both nearly equal in diameter. The journal is mounted on the external race of a rolling element bearing and prevented from spinning with loose pins or a squirrel cage that provides a centering elastic mechanism. Between the journal and housing, the annular squeeze film, typically ~ ¼ mm or so, is filled with a lubricant provided as a splash from the rolling element bearing lubrication system or by a dedicated pressurized delivery. In operation, as the journal moves due to dynamic forces acting on the system, the fluid is displaced to accommodate these motions. As a result, hydrodynamic squeeze film pressures exert reaction forces on the journal and provide for a mechanism to attenuate transmitted forces and to reduce the rotor amplitude of motion.

In practice SFDs operate with low magnitudes of oil feed pressure (5 bar max.) that generally do not prevent the lubricant in the fluid film lands from liquid vaporization or entrainment of external gaseous media into the film lands. Open ends SFDs or SFDs sealed with piston rings (and end plate seals) are prone to develop a flow regime where the ingestion and entrainment of air leads to the formation of a bubbly lubricant. This is a mixture of two distinct fluids, one viscous and quite dense, and the other much less viscous and light.

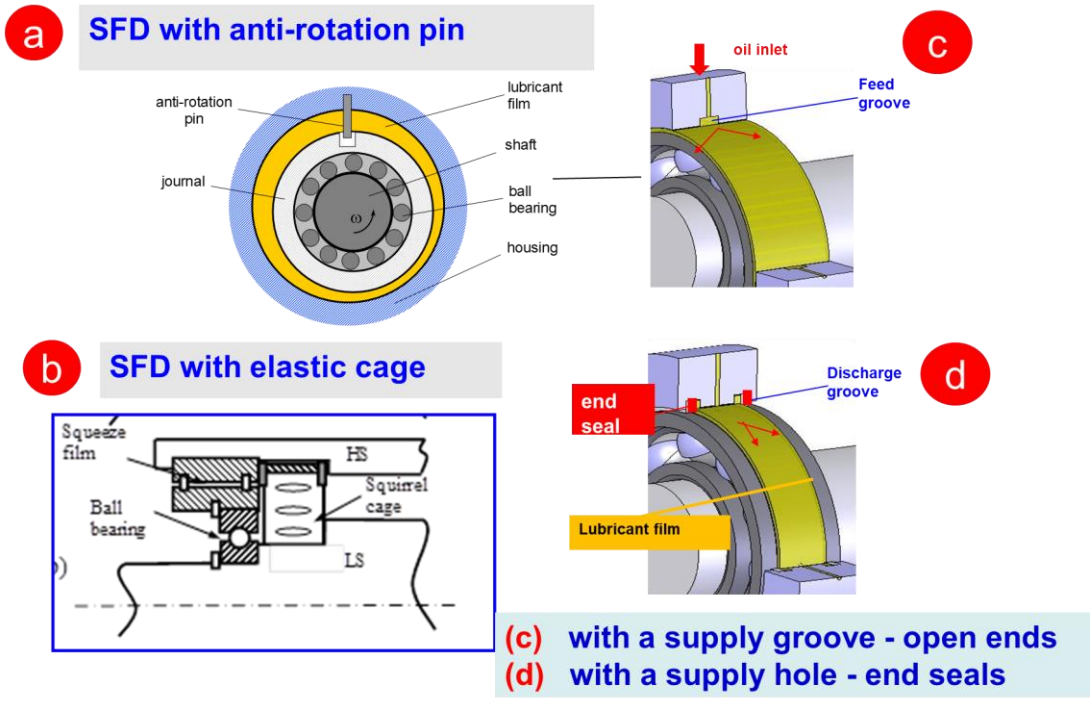

Fig 1. Typical squeeze film damper (SFD) configurations.

Figure 2 shows conceptual views of intershaft dampers for multiple-spool gas turbine engines. These dampers are subject to whirl motions resulting from the combined imbalance response of both low speed (LS) and high speed (HS) rotors. Most SFDs in US aircraft engines incorporate the arrangements in Figure 2(a & b) where the journal (and rolling element bearing) is elastically supported, and the bearing is rigidly attached to the engine frame. The (soft) spring support and SFD *see* the same deflections though the dynamic loads do not divide equally between them.

Dampers in jet engines operate with low values of external pressurization (2 or 3 bar max.) to avoid excessive weight and volume in the lubrication system. Note also that most aircraft engines do not use any type of hydrodynamic journal bearings to avoid the risk of fluid film bearing induced instabilities. (However, in some dual shaft jet engines, the inter-spool fluid film bearing, shown in Figure 2a, is known to be a source of such instabilities).

The amount of damping produced is the critical design consideration. If damping is too large, the SFD acts as a rigid constraint to the rotor-bearing system with large forces transmitted to the supporting structure. If damping is too light, the damper is ineffective and likely to permit large amplitudes of vibratory motion with likely subsynchronous motions. Note also that, to be effective, a damping element must be "soft" to allow for motions (or displacements) at the location of the support, in particular while crossing natural vibratory modes.

The damper geometry (length L, diameter D, and clearance c), operating whirl frequency, and fluid physical properties (density and viscosity) determine, on first instance, the dynamic forced performance of SFDs. However, there are other important considerations that ultimately determine an appropriate operation. The relevant issues are:

a) kinematics of journal (tied to rotor system and acting forces), in particular the squeeze film velocity ~ amplitude of motion (r) x whirl frequency (ω).
b) magnitude of lubricant supply pressure for adequate flow rate and cooling,
c) feeding (holes and/or grooves) and end sealing arrangements (O-ings, piston rings, etc.)
d) fluid inertia effects,
e) flow condition, laminar or turbulent.
f) type of lubricant dynamic cavitation (vapor or gaseous) and air ingestion and entrapment.

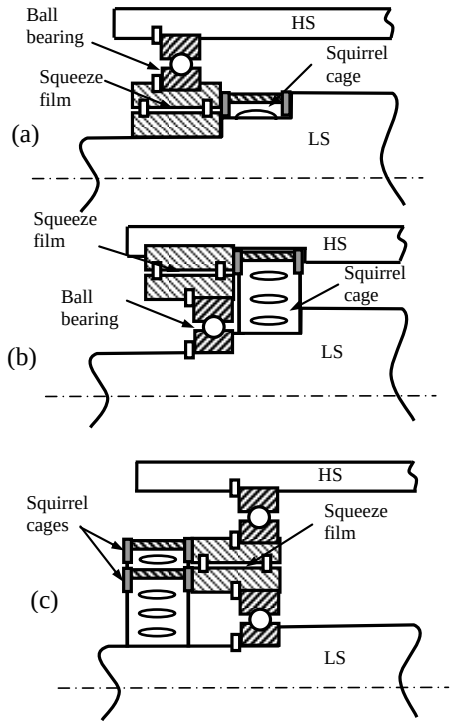

Fig. 2 Schematic views of intershaft damper configurations: (a) squeeze film rotates with low speed (LS) rotor, (b) squeeze film rotates with high speed (HS) rotor, and (c) double ball bearing-squirrel cage design.

Models for the Performance of SFDs

In actual practice most dampers are short in axial length, $L/D < 0.50$, and accommodate some type of end seals to increase their damping capability. SFDs include additional features such as high resistance orifices for pressure delivery and discharge and/or deep grooves acting as flow sources or sinks of uniform pressure.

SFD reaction forces and force coefficients are conveniently divided into two major types related to the specific journal center kinematics. For imbalance response analyses, SFD forces are obtained under the assumption of circular centered orbits. The model is applicable when the rotor traverses a critical speed, for example, where the imbalance "force" induces large amplitude orbital motions as the system may have little damping. On the other hand, for rotordynamic critical speed and stability analyses, SFD force coefficients are obtained for small amplitude, journal center motions about a static (equilibrium) position. In the 21st century, computational tools analyze rotor-bearing system transient response events by considering the instantaneous SFD reaction forces, a function of time varying journal kinematics.

Figure 3 depicts a schematic view of a journal whirling within its bearing of radius R (= ½ D) and length L. Lubricant of density ρ and viscosity μ fills the radial clearance c between the bearing and its journal. As the journal whirls, it squeezes the film thickness h, displaces the fluid and generates a pressure field. The film thickness equals

$$h = c + [\, e_{Xo} + \Delta e_{X(t)}] \cos\Theta + [\, e_{Yo} + \Delta e_{Y(t)}] \sin\Theta] \tag{1}$$

where (e_{Xo}, e_{Yo}) and $(\Delta e_X, \Delta e_Y)_{(t)}$ are the static and dynamic components of journal motion, respectively. In Fig. 3, Θ and z denote circumferential and axial coordinates attached to the bearing surfaces; and (X,Y) is a fixed coordinate system for description of the journal kinematics. In operation, the journal motions have a whirl frequency (ω) coinciding with the rotor speed, i.e., synchronous excitation from rotor imbalance, for example.

Unlike conventional oil lubricated journal bearings, fluid inertia affects the forced performance of SFDs due to their typically large clearances and operation at high frequencies [1]. The squeeze film Reynolds number $Re_s=(\rho/\mu)\omega c^2$ ranges from one to 50 in most practical applications. Fluid inertia effects are relevant in dampers with large clearances, using light viscous lubricants, and operating at high frequencies, say above 6 krpm (100 Hz). In general, large clearance SFDs generate significant direct added mass coefficients that may significantly lower the critical speeds of compact rotating machinery, as in some small size jet engine applications [2].

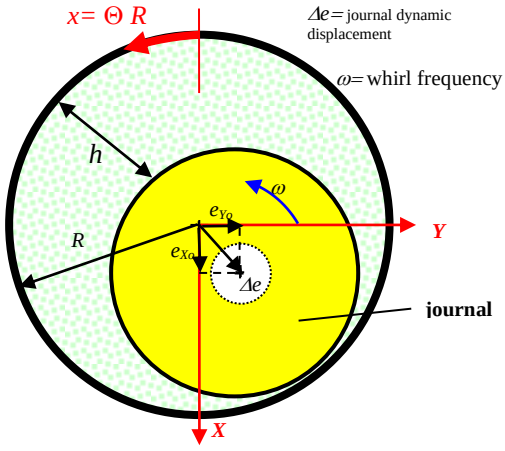

Fig. 3 View of whirling journal and coordinate system for analysis.

Considering only temporal fluid inertia[2], the equation governing the generation of dynamic pressure P is: [9]

$$\frac{\partial}{R\partial\Theta}\left(h^3\frac{\partial P}{R\partial\Theta}\right)+\frac{\partial}{\partial z}\left(h^3\frac{\partial P}{\partial z}\right)=12\,\mu\frac{\partial h}{\partial t}+\left(\rho h^2\right)\frac{\partial^2 h}{\partial t^2} \tag{2}$$

Eq. (2) is an updated form of the classical Reynolds Eq. [2,3] that adds the effect of temporal fluid inertia. On the right-hand side of Eq. (2), the first term represents the squeeze film action due to the journal center velocity, and the second term denotes the effects of the journal acceleration. Above,

$$\partial h/\partial t = [V_X \cos\Theta + V_Y \sin\Theta], \text{ and } \partial^2 h/\partial t^2 = [A_X \cos\Theta + A_Y \sin\Theta] \tag{3}$$

where $(V_X, V_Y) = d\Delta e_X/dt,\ d\Delta e_Y/dt)$ and $(A_X, A_Y) = (d^2\Delta e_X/dt^2,\ d^2\Delta e_Y/dt^2)$ are the components of the journal center velocity and acceleration, respectively.

Numerical solutions to Eqn. (2) with specific boundary conditions and accounting for lubricant cavitation (vapor or gas) are readily available, see Ref. [8,9]. Detailed physics-based solutions modeling air ingestion and entrapment have recently appeared; see Refs. [10,11]. Ref. [12] (2022) conveniently copies the SFD models introduced in Refs. [8,9,10]. Persistent air ingestion makes the damper operate with a bubbly mixture (foam like). The physical phenomenon is exceedingly complex, only understood in a time ensemble averaged manner.

By 2024, numerical predictions of SFD performance based on commercial computational fluid mechanics (CFD) software have appeared; for example see Ref. [13]. Alas the predictions are often off the mark when compared to test data and do not justify the exceptional computing time and engineering effort.

Once found a solution to the elliptical Eq. (2) with appropriate boundary conditions, the integration of the pressure field on the journal surface produces reaction forces,

$$\begin{Bmatrix} F_X \\ F_Y \end{Bmatrix} = -\int_{-L/2}^{L/2}\int_0^{2\pi} P_{(\theta,z,t)} \begin{Bmatrix} \cos\theta \\ \sin\theta \end{Bmatrix} R\,d\theta\,dz \tag{4}$$

SFD dynamic force coefficients for small amplitude motions

SFD reaction forces due to small amplitude journal center motions about a static eccentric or off-centered position defined as $e_{Xo}=e_s$ and $e_{Yo}=0$, as shown in Fig. 4, are of importance in the evaluation of natural frequencies and stability of rotor-bearing systems mounted on dampers with soft or no centering springs. The damper forces are represented in the linearized form,

[2] Fluid advection, the transport of a property by the fluid motion, is also important albeit leading to nonlinear fluid momentum and continuity equations, not a simple Reynolds-like equation. See Ref. [14] (1987) for a pioneering original computational effort, well before the advent of fast-speed computing. The reference also includes Eq. (2) as a limit case for speedy calculation.

$$\begin{bmatrix} F_X \\ F_Y \end{bmatrix} = -\begin{bmatrix} C_{XX} & C_{XY} \\ C_{YX} & C_{YY} \end{bmatrix}\begin{bmatrix} V_X \\ V_Y \end{bmatrix} - \begin{bmatrix} M_{XX} & M_{XY} \\ M_{YX} & M_{YY} \end{bmatrix}\begin{bmatrix} A_X \\ A_Y \end{bmatrix} \tag{5}$$

where (V_X, V_Y) and (A_X, A_Y) are the instantaneous journal center velocities and accelerations along the X and Y directions, respectively. ($C_{\alpha\beta}$, $M_{\alpha\beta}$) $_{\alpha\beta=X,Y}$ are the damping and inertia (rotordynamic) force coefficients[3], respectively. Recall that a SFD does not produce direct stiffnesses. That is, without journal spinning and at a fixed journal static eccentricity, a damper cannot generate a pressure field (P=0), hence the static reaction force F = 0.

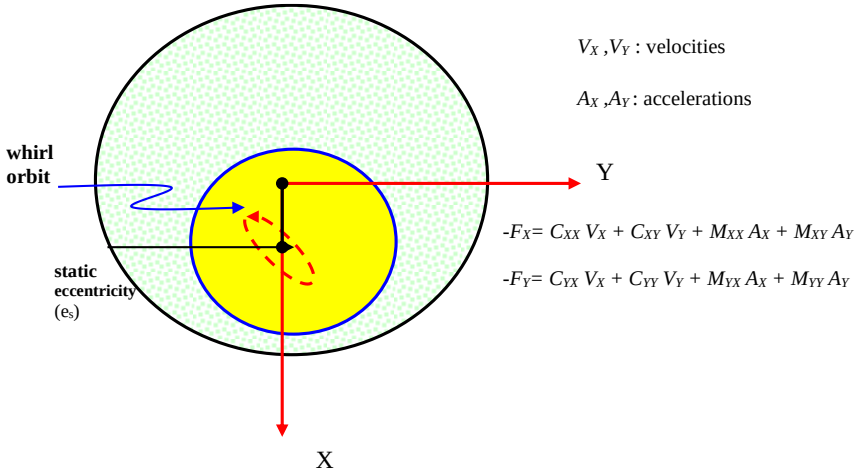

Fig. 4. SFD model: small amplitude journal motions about static off-centered position (e_S).

Table 1 lists formulas for the linearized force coefficients of a short length (L/D < 0.33), open ends SFD. The coefficients are nonlinear functions of the static journal eccentricity ($\varepsilon = e_s/c$). The fluid inertia or added mass coefficients are strictly valid for small to moderate squeeze film Reynolds numbers, $\mathrm{Re}_s=(\rho/\mu)\omega\, c^2 < 10$.

Table 1. Linearized force coefficients for open ends SFD

(STRICTLY VALID) Small amplitude motions about a journal **off-center static** position $\varepsilon=e_s/c$. Source Refs. [1,2]

Full film model (No oil cavitation)	**π-Film Model (Cavitated) (*)**
$C_{XX} = \mu D\left(\frac{L}{c}\right)^3 \frac{\pi\left(1+2\varepsilon^2\right)}{2\left(1-\varepsilon^2\right)^2},\ C_{XY}=0$	$C_{XX} = \mu D\left(\frac{L}{c}\right)^3 \frac{\pi}{2}\frac{\left[3\varepsilon + i\,\frac{\left(1+2\varepsilon^2\right)}{2}\right]}{2\left(1-\varepsilon^2\right)^2},\ C_{XY} = \mu D\left(\frac{L}{c}\right)^3 \frac{\varepsilon}{\left(1-\varepsilon^2\right)^2}$
$C_{YY} = \mu D\left(\frac{L}{c}\right)^3 \frac{\pi}{2\left(1-\varepsilon^2\right)^{3/2}},\ C_{YX}=0$	$C_{YY} = \mu D\left(\frac{L}{c}\right)^3 \frac{\pi}{4\left(1-\varepsilon^2\right)^{3/2}},\ C_{YX}=0$
$M_{XX} = \rho D\left(\frac{L^3}{c}\right)\frac{\alpha\pi\left[1-\left(1-\varepsilon^2\right)^{1/2}\right]}{12\,\varepsilon^2\left(1-\varepsilon^2\right)^{1/2}},\ M_{XY}=0$	$M_{XX} = \rho D\left(\frac{L^3}{c}\right)\frac{\alpha\,(i-\pi-2\varepsilon)}{24\,\varepsilon^2},\ M_{XY} = \rho D\left(\frac{L^3}{c}\right)\frac{\alpha\left[\ln\left\{\frac{(1-\varepsilon)}{(1+\varepsilon)}\right\}-2\varepsilon\right]}{24\,\varepsilon^2}$
$M_{YY} = \rho D\left(\frac{L^3}{c}\right)\frac{\alpha\ \pi\left[1-\left(1-\varepsilon^2\right)^{1/2}\right]}{12\,\varepsilon^2},\ M_{XY}=0$	$M_{YY} = \rho D\left(\frac{L^3}{c}\right)\frac{\alpha\ \pi\left[1-\left(1-\varepsilon^2\right)^{1/2}\right]}{24\,\varepsilon^2},\ M_{XY}=0$

$i = \frac{2\cos(-\varepsilon)}{\left(1-\varepsilon^2\right)^{1/2}}$, and α = 1.2-1.0 for small to moderately large squeeze film Reynolds numbers (Re_s < 50). Note C_{YX} and M_{YX} are nil.

(*) Take with caution the force coefficients for the π-film damper since oil cavitation (vapor or gas) does not occur for (very) small amplitude journal motions.

[3] These force coefficients represent changes in forces due to small changes in motion amplitude. This condition may not be applicable to SFDs as they must displace a finite distance to work effectively.

For an open ends damper with L=63.5 mm, D=127 mm, c=0.137 mm and lubricated with a light oil (μ= 2.14 10^{-3} Pa.s, ρ=785 kg/m^3), Figure 5 depicts the damping and inertia force coefficients. Recall that these coefficients are derived for small amplitude motions about a static eccentric position ($e_s = e_X$). Note that L/D=0.5, i.e., the geometry does not represent strictly a short length damper. The force coefficients grow rapidly with e_s, i.e., they appear highly nonlinear. Note that $C_{XX} > C_{YY,}$ $M_{XX} > M_{YY}$; $C_{XY} = C_{YX}$=0; and $M_{XY} = M_{YX}$=0. Both damping and inertia force coefficients are nonlinear, growing rapidly with the (static) eccentricity (e_X/c). Most importantly, the added mass coefficients are large in magnitude; M_{XX}. $M_{YY} > \sim 24.4$ kg. Consider that the mass of fluid in the annular film region is just ($\pi\rho DLc$)=2.72 gram!

As noted early, the force coefficients in Table 1 are useful for the stability analysis of a rotor-bearing/SFD system. These coefficients are not intended to represent SFDs undergoing large amplitude journal motions, for example a sizeable fraction of the damper clearance.

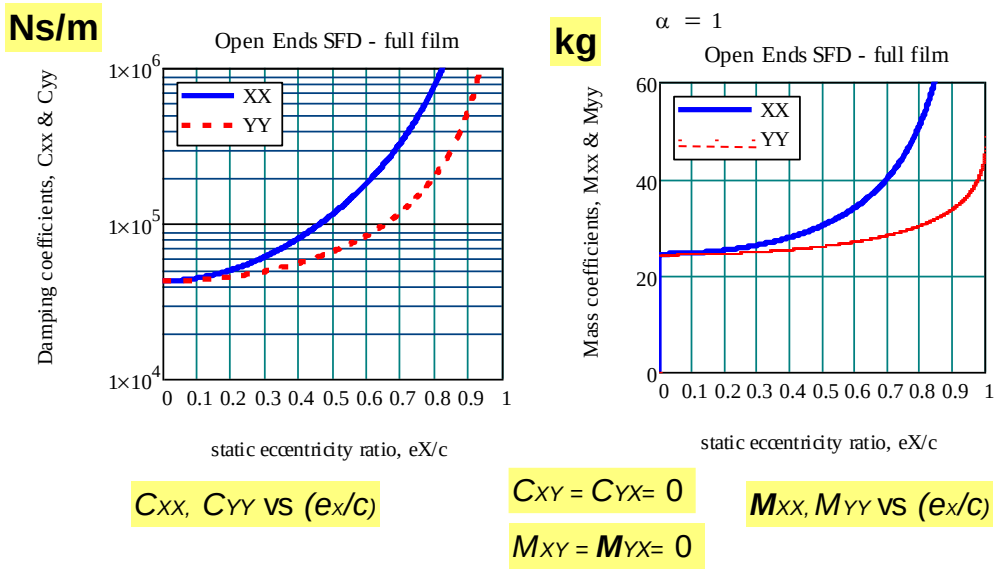

Fig. 5. Open ends (short length) SFD: example of damping and inertia force coefficients. Small amplitude motions about off-centered journal static position (full film model).

Open Ends SFD dynamic force coefficients for circular orbits

SFDs to be effective must displace dynamically to generate dissipative (damping) forces. The journal or rotor motions are not typically (infinitesimally) small in amplitude but rather large, a sizeable fraction of the film clearance. This condition is particular to operation when a rotor traverses a critical speed, and the excitation source is the rotor mass imbalance.

Figure 6 shows a SFD journal describing circular centered orbits of amplitude *(e)* and whirl frequency *(ω)*. The damper generates a constant reaction film force in a reference frame rotating with frequency ω. The radial *(F_r)* and tangential *(F_t)* components of the damper reaction force are:

$$F_r = -\{C_{rt} V_t + M_{rr} A_r\}; \quad F_t = -\{C_{tt} V_t + M_{tr} A_r\} \tag{6}$$

where $V_t = e\omega$ and $A_r = -e\omega^2$ are the journal center tangential speed and radial acceleration, respectively. $V_t = (e\omega)$ is also known as a squeeze film velocity. (C_{tt}, C_{rt}) are the direct and cross-coupled damping coefficients, and (M_{rr}, M_{tr}) are added mass coefficients, respectively. Please remember the idealized SFD does not generate a stiffness (K), i.e., a reaction force due to a static journal displacement. The archival literature misleads the practicing engineering when referring to a damper having a radial stiffness K_{rr} = (C_{rt} ω), that is frequency dependent [2]

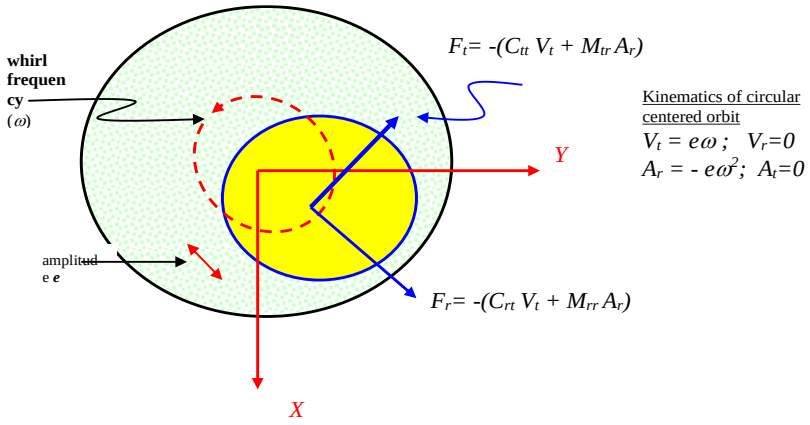

Fig. 6 SFD performing circular centered orbits with amplitude *e* and frequency *ω*.

For the short-length, open ends *SFD* model, the force coefficients using the rather simplistic π-film assumption (i.e. half the damper circumference develops film cavitation) are [2]

$$C_{tt} = \frac{\pi \mu D}{4\left(1-\varepsilon^2\right)^{3/2}}\left(\frac{L}{c}\right)^3 ;\; C_{rt} = \frac{\mu\, \varepsilon\, D}{\left(1-\varepsilon^2\right)^2}\left(\frac{L}{c}\right)^3 \tag{7a}$$

$$M_{rr} = \frac{\pi \rho D}{24}\left(\frac{L^3}{c}\right)\left[1-2\left(1-\varepsilon^2\right)^{1/2}\right]\left\{\frac{\left(1-\varepsilon^2\right)^{1/2}-1}{\varepsilon^2\left(1-\varepsilon^2\right)^{1/2}}\right\}; \tag{7b}$$

$$M_{tr} = -\frac{27}{140\,\varepsilon}\,\rho D\left(\frac{L^3}{c}\right)\left[2+\frac{1}{\varepsilon}\ln\left(\frac{1-\varepsilon}{1+\varepsilon}\right)\right]$$

where *(L, D, c)* denote the damper axial length, diameter, and radial clearance, respectively, and $\varepsilon = e/c$ is the dimensionless orbit radius. The orbit radius *(e)* should not be confused with the static journal offset displacement; (e_s =0) null in this case. Note that the coefficients in Eq. (7) are not strictly rotordynamic coefficients as their classical definition implies small amplitude motions (perturbations) about a journal equilibrium position. Incidentally, the physical model and resulting Eqs. (7) dispense with the means of providing lubricant to the squeeze film section, either via a central groove or through orifices. The idealized SFD is not practical.

The coefficients above are determined under the assumptions of an isoviscous and incompressible lubricant that is supplied with a low (unspecified) supply pressure. Most importantly, the model assumes a squeeze film fully submerged in a lubricant bath. That is, a liquid media surrounds the exit sections of the damper, not a gas or ambient air.

For the full film model (no oil cavitation), the direct coefficients (C_{tt}, M_{rr}) equal twice those in Eq. (7), while the cross-coupled coefficients (C_{rt}, M_{tr})=0. The inertia force coefficients are strictly valid for $\mathrm{Re}_s = (\rho/\mu)\omega\, c^2 < 10$. The full film coefficients are more realistic, in particular for circular motions of small amplitude ($e < ¼\, c$) about the bearing center.

Figure 7 shows the damping and inertia force coefficients for a short length, open ends SFD describing circular centered orbits *(*CCOs*)*. The damper length L=50 mm, c=0.080 mm, L/D=0.25, with lubricant viscosity and density (μ,ρ) equal to 20 cPoise and 890 kg/m^3, respectively. The predicted force coefficients are highly nonlinear functions of the orbit radius *(e).*

For the example, the mass of a steel journal with the dimensions noted $M_J = \rho_s\, \pi R^2 L$ = 12.25 kg and the fluid mass in the film equals $M_o = \rho\pi DLc$ = 22 gram. The added or virtual mass coefficient M_{rr} ~ 1.90 kg, orders of magnitude larger than the physical mass of the liquid in the film, and of the same order of magnitude as the mass of the steel journal. The inertia force coefficients (M_{rr}, M_{rt}) influence the system rotordynamic response, despite that the fluid mass M_o is just a few grams. Hence, fluid inertia in SFDs impacts the location of critical speeds in compact rotors operating at high rotational speeds. The effect is stronger (amplified) for dampers configured with tight end seals.

Note the large magnitudes of direct damping (C_{tt}) even for motions around the centered position (e=0). The rapid growth of the cross-coupled damping coefficient (C_{rt}) is referred as a "stiffness hardening effect" since $K_{rr} = C_{rt}\, \omega$. K_{rr} is the culprit of severe nonlinear (multiple valued) rotor response accompanied with jump-phenomenon and orbit-instability. However, these effects, mostly predicted by overly simplified theoretical analyses, are hardly ever reported to occur in practice.

In actual operation, air entrainment is most prevalent for large amplitude orbital motions $(e \rightarrow c)$ and high frequencies of

operation, i.e. under large squeeze velocities ($V_t = e\omega$) that produce a damper forced response quite distinct from the one derived with the (highly nonlinear) force coefficients shown in Eqs. (5,6).

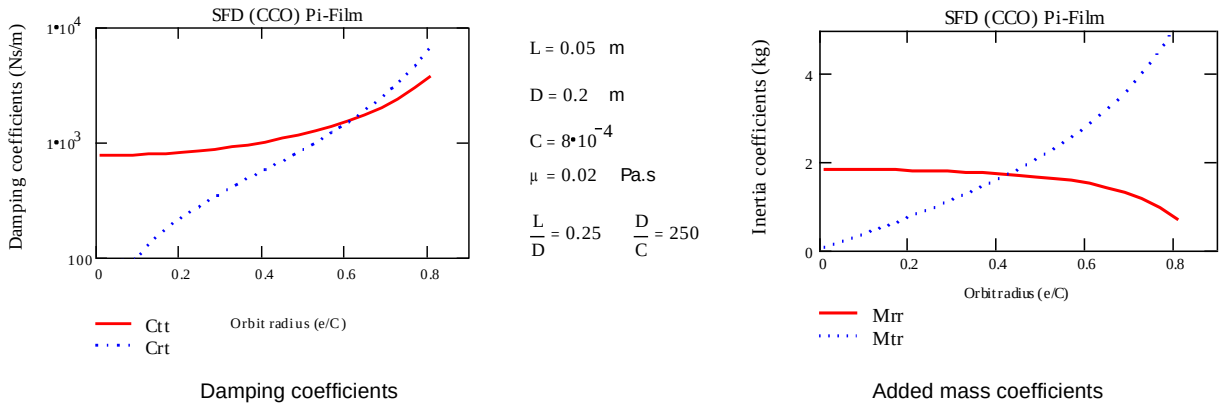

Fig. 7. Open ends SFD force coefficients for circular centered motions (π film model). Example

In operation, stiffness hardening (K_{rr} >>0) is most likely due to contact and rubbing of the journal against the bearing. This many happen as the rotor traverses a critical speed with large amplitude orbital motions due to little damping or excessive rotor imbalance, for example. In these events, damper forces are negligible since the fluid film is probably ruptured with large amounts of air entrainment. Thus, rotor-SFD dynamic response models based on the π-film SFD model have little relationship with actual rotor responses.

There are also equations applicable to finite length SFDs. For small amplitude motions (orbit radius e/c < 0.25), the SFD force coefficients for a full film, open ends SFD are:

$$C_{XX} = C_{YY} = C_{tt} = 12\pi \frac{\mu R^3 L}{c^3}\left[1 - \frac{\tanh\left(L/D\right)}{\left(L/D\right)}\right] \qquad M_{XX} = M_{XX} = M_{rr} = \pi \frac{\rho R^3 L}{c}\left[1 - \frac{\tanh\left(L/D\right)}{\left(L/D\right)}\right] \tag{8}$$

as first derived by Reinhart and Lund [15] (1975) and reproduced by San Andrés [16] in 1985.

Note that the damping coefficient is proportional to $1/c^3$ while the inertia coefficient varies with $1/c$. Contrary to a long-held assumption, the added mass coefficient is ever present; that is, it is a physical property of the mechanical system. Its influence on the dynamics of a rotor-bearing system, however, becomes dominant at high frequencies, i.e., when the rotor accelerations ($A_r = -e\omega^2$) are large. At these operating conditions, the inertia forces $|M_{rr} A_r|$ are of the same order or even larger than the viscous (damping) force $|C_{tt} V_t|$, where $V_t = (e\omega)$ is the squeeze velocity.

There is good correlation between experimental and predicted force coefficients for *SFDs* operating with circular centered orbits, see Ref. [17] (1996). The test damping coefficients *(C_{tt}, C_{rt})* fall in between the π- and full-film predictions. At low frequencies, the oil cavitation zone does not extend over half the damper circumference, and thus the damping coefficients approach the full film predictions. On the other hand, as the whirl frequency increases so does the squeeze film pressure and the cavitation zone extends. The experimental coefficients thus approach those derived for the π-film model.

It is most important to note that the experiments in [17] were conducted with a damper fully submerged in a lubricant bath. The test rig closed any paths that would permit the natural ingestion and entrapment of air. This condition in practice is most difficult to achieve. San Andrés and Delgado [18] (2007) and [19] (2010) present more experimental damping coefficients along with predictions, see Figure 8.

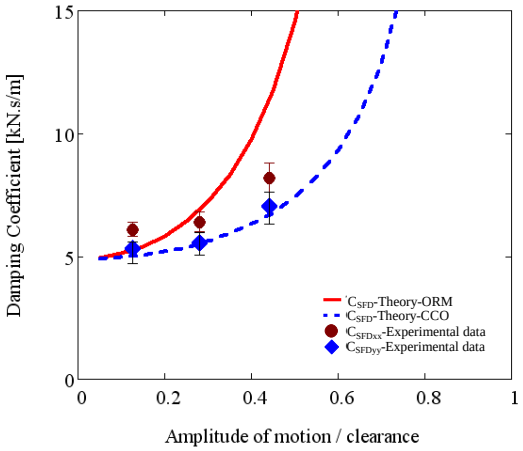

Fig. 8. Open SFD damping coefficients vs. orbit amplitude. Predictions for circular centered orbits (CCO) and motions about an off-centered static position (ORM). Data from [19] (2010).

The effect of air entrainment on squeeze film pressures and damper reaction forces has been thoroughly researched qualitatively and quantitatively since the mid-1990s. Refs. [8] (2003) and [10] (2022) report fundamental experimental results and advance an analytical model for this prevalent operating condition. Please see later a further discussion on this important issue. A brief discussion follows on other geometrical configurations and operating conditions that affect the performance of SFDs.

Effect of feed grooves on SFD force performance

Some dampers are designed with feed and discharge grooves to ensure a continuous flow of lubricant through the squeeze film lands, see Figure 9 for a schematic view. A groove is thought to provide a uniform flow source with constant pressure around the bearing circumference. A central feed groove also divides the flow region into two separate squeeze film dampers working in parallel, i.e. the reaction forces from each land add.

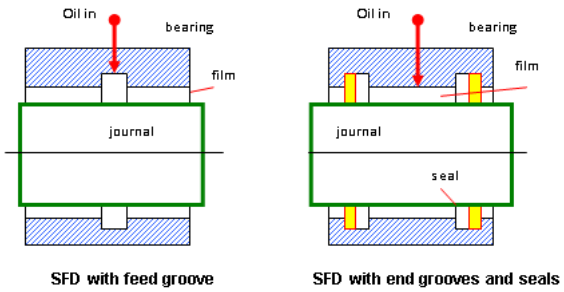

Fig. 9 SFD typical grooved configurations: with central groove and side grooves for seals installation.

For the open ends FD with a central groove SFD and having two adjacent film lands of length L, theory predicts forces about one-fourth those from a SFD with twice the land length (=2L) and no groove. This is so since the damper reaction force for the no groove configuration ~ $(2L)^3$ whereas the force for the grooved damper ~ $2L^3$.

Experiments and field performance, however, demonstrate that grooved dampers generate much larger magnitudes of force than those derived from the simple theory. Large amplitude dynamic pressures are measured at the groove regions connecting the two squeeze film regions. Thus, a central groove does not isolate the adjacent film lands, but rather interacts with the squeeze film regions. See Refs. [16] (1985), [20] (1997), [21] (2007), and [6] (2016). Figure 10 shows a schematic view of the flow region that includes a deep feed groove and adjacent film lands. The figure includes measured dynamic pressures in the groove that are as large as those in the thin film section.

Ref. [9] (2010) presents an original model for prediction of the forced response of grooved SFDs and oil seal rings with internal grooves. The model includes fluid inertia and account for the flow interaction at the groove-film land interface that amplifies the generation of squeeze film pressures. The model predictions based on an effective grove depth are in good

agreement with measured stiffness, damping and inertia force coefficients in oil seal rings with multiple internal cavities, presented in Ref. (21) [2007], and in dampers with both inlet and discharge deep grooves, shown in Ref. (20) [1997]. The effective groove depth ranges from 5 to 20 x film clearance (c), irrespective of the groove actual physical depth which could be two or more orders of magnitude larger than the clearance. Gheller et al. [12] (2022) reproduce the original model of Delgado and San Andrés [9] (2010) but do to notice the significance of the effective depth.

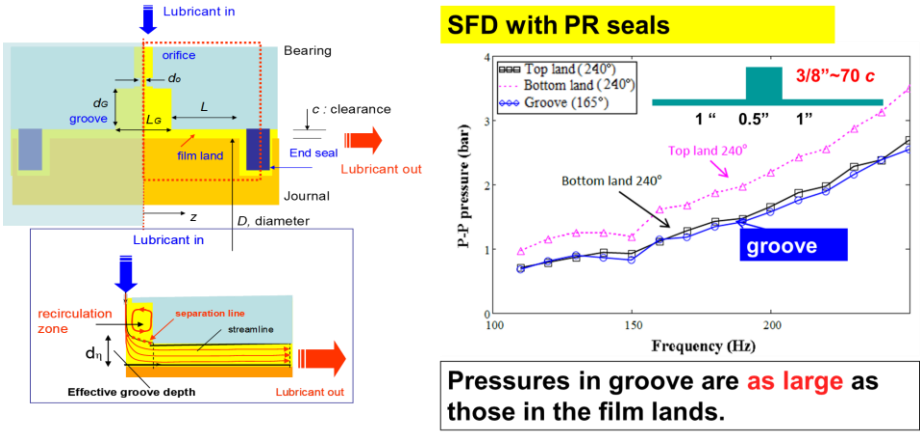

Fig. 10 SFD with a central feed groove and measure film and groove pressures. Data reproduced from Ref. [6]

Effect of end seals on SFD force performance

SFDs usually include some type of end seals to reduce the through flow and to amplify the viscous damping. The most common end seal configurations include O-rings, piston rings, and end plate (clearance gap) seals, all depicted schematically in Figure 11. Measurements and analysis show larger forces for the end-sealed condition, although the lubricant can rapidly heat (and lower the oil viscosity) for designs with small through flows.

SFDs in commercial jet engine rotors incorporate piston rings as end seals (O-rings for military engines) [6]. However, ring cocking and locking with a resulting excessive oil leakage is a pervasive problem. Implementing patented (proprietary) designs seems to resolve the reliability issue, see Ref. [9] (2016).

Many industrial compressor applications also implement O-ring end seals due to their ready availability and tight sealing. However, these applications are restricted to low static loads and low temperatures. Material compatibility of the O-rings with the lubricant and gas external medium is a design consideration. Aging, temperature degradation, long-term relaxation, and creep of the elastomeric O-rings, when supporting large static loads, are issues usually overlooked. The oversight can prove fatal.

Formulas for the prediction of SFD force coefficients with tight end seals (large flow resistance) can be easily derived from the Reinhart and Lund Eqs. (7) by assuming an infinitely long bearing ($L/D >> 0$). In this case, the squeeze film pressure does not vary axially, and the damper produces a large reaction force despite the limited physical length. In the limit, the damping and virtual mass coefficients for a fully sealed SFD are:

$$C_{XX}=C_{YY}=C_{tt}= 12\,\pi\,\mu\,(R/c)^3\,L; \quad M_{XX}=M_{YY}=M_{rr}=\pi\,\rho\,R^3\,L/c \tag{9}$$

These coefficients are valid for small amplitude motions about the bearing center (e=0) and a full film condition (no lubricant cavitation).

From Eq. (7), the force coefficients for the full film, open ends (short length) SFD and e=0 are $C_{XX}=C_{YY}=C_{tt}= \frac{1}{2}\,\pi\,\mu\,D(L/c)^3$ and $M_{XX}=M_{YY}=M_{rr}= 1/24\,\pi\,\rho\,D(L^3/c)$. Hence, the ratio of force coefficients (sealed/open) equals

$$C_{tt\_sealed}/C_{tt\_open} = M_{rr\_sealed}/M_{rr\_open} = 3(D/L)^2 \tag{10}$$

That is, for a damper with L/D=1/5, a fully sealed construction can amplify the damping coefficient by (3 x 5^2) = 75 times when compared to the open ends configuration! At the same time, however, the added mass coefficient increases in an identical proportion.

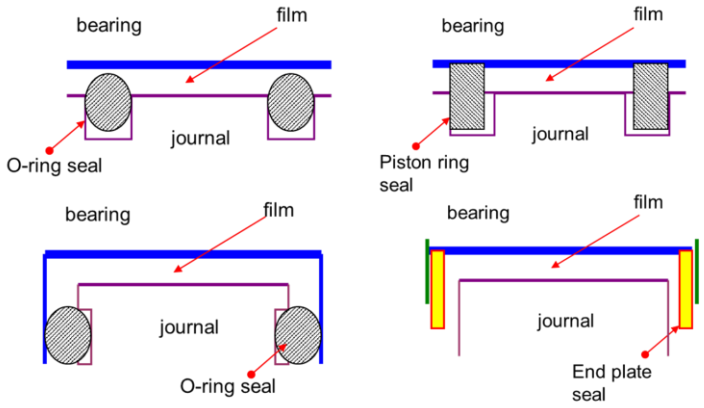

Fig. 11 Types on end seals in SFDs: O-rings, piston rings, and end plate seals.

The design of end seals demands empirical seal coefficients (C_{seal}) that are extracted from exhaustive experimentation. In general, an end seal restriction is modeled as a resistance to the local exit flow (q_{end}), and such that is proportional to the pressure drop across, i.e., $q_{end} = (1/R_f)\, \Delta P|_{z=end} = C_{seal}\, \Delta P_{end}$, with C_{seal} representing a local flow conductance in units of [(m_2/s)/Pa]. In short, C_{seal}=0 makes a very tight end seal without side flow, whereas $1/C_{seal} \rightarrow 0$ represents an open ends condition.

Until recently, experience dictated the best type of sealing to be implemented. Extensive experimentation conducted for an aircraft engine company [6] (2016) allowed for substantial progress and sound theoretical developments. Recently, San Andrés and Koo [10] (2020) and [11] (2023) introduce a two-way orifice-like model for the flow through a piston ring slit and validate predictions against experimental data which evidenced persistent air ingestion for too low lubricant pressure supplies.

Lubricant cavitation vs. air ingestion and entrapment in SFDS

Zeidan et al. [4] (1996) identify SFD operation with distinct types of dynamic fluid cavitation (vapor or gas), and a regime due to air ingestion and entrapment. The appearance of a particular condition depends on the damper type (sealed ends or open to ambient), the levels of supply pressure and flow rate, whirl frequency (ω), and the magnitude of dynamic load producing (small or large) journal displacements ($e_{(t)}$) within the film clearance. The squeeze film velocity ($e\omega$) is the most important kinematics parameter.

Gas cavitation following the journal motion appears in ventilated (open ends) SFDs operating at low frequencies and with small to moderate journal amplitude motions, i.e., small ($e\omega$). A well-defined cavitation *bubble* containing the release of dissolved gas in the lubricant or air entrained from the vented sides follows the whirling motion of the journal. In other words, the cavitation zone appears steady in a rotating frame. The traveling gas bubble appears not to affect the generation of the squeeze film pressure in the full film zone. The persistence of this cavitation regime upon reaching steady operating conditions (high frequencies) in an aircraft application is remote.

Lubricant vapor cavitation appears in dampers with tight end seals that prevent entrainment of the external gas media and for operation with a sufficiently large supply pressure. In this last case, the through oil flow also prevents the ingestion of air. Furthermore, the lubricant must be relatively free of dissolved gases such as air, a condition not readily found in practice.

Figure 12(a) depicts the measured dynamic film pressure wave vs. time in a damper that has developed lubricant vapor cavitation. Taken from Ref. [22] (2001), the graphs illustrate the variation of dynamic squeeze film pressure and gap (film thickness) for five periods of journal orbital motion. The damper radial clearance is c=0.343 mm. The whirl frequency ω=75 Hz, and the centered journal orbital amplitude e=0.180 mm=0.52 c. The squeeze film velocity is ($e\omega$) =85 mm/s. The oil supply pressure is 1.45 bar and the discharge is ambient to a pool of liquid. That is, the damper is fully submerged in a lubricant bath. Note that the pressure profile is smooth and shows nearly identical shapes for each consecutive period of motion. A (flat) constant pressure zone develops at nearly zero absolute pressure, and it corresponds to the rupture of the film and formation of a vapor filled cavity. The cavity appears only during that portion of the journal motion cycle where the film gap increases. The vapor bubble collapses immediately as the local pressure rises above the lubricant vapor pressure. In general, correlations of measured pressures and vapor cavitation extent with predictions based on traditional film rupture models are satisfactory; see the fundamental work of Diaz and San Andrés [22] (2001).

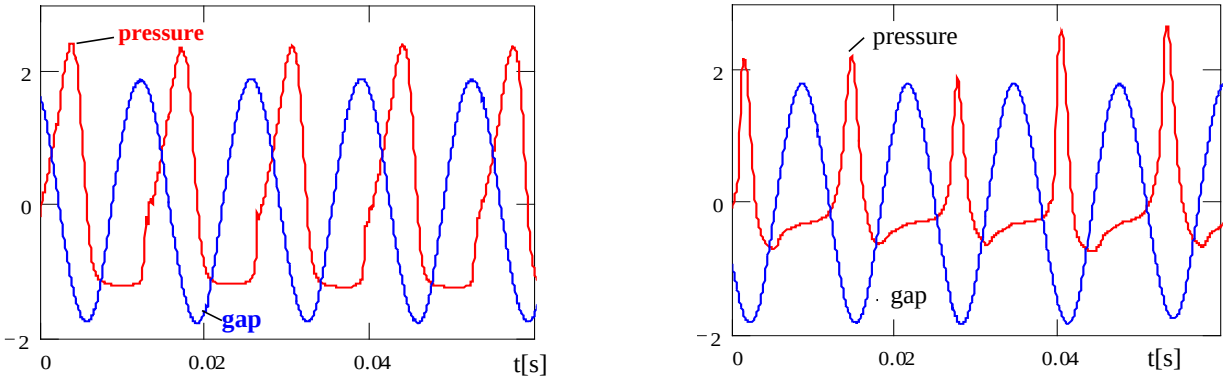

(a) Flooded SFD: Vapor cavitation **(b) Open SFD: Air ingestion and entrapment**

Fig. 12 Dynamic film pressure (bar) and local film gap (mm x 10). (a) flooded SFD with vapor cavitation, (b) SFD venting to air and pressure profile showing air ingestion. Taken from Ref. [22]

Air ingestion and entrapment appear and persist in vented (or open ends) dampers operating at high frequencies and with low magnitudes of supply (feed) pressure, i.e. small throughout flow rates. Figure 13(b) depicts the measured film pressure versus time in a SFD with air entrainment. The operating conditions are identical to those for the measurements depicted in Figure 13(a), except that the damper is open to ambient conditions, i.e., not submerged in an oil bath. A suction pressure draws air into the thin film at the locations where the local film gap is increasing. The cyclic fluid motion leads to air entrapment, with bubbles remaining in the zones of dynamic pressure generation above ambient. Air ingestion leads to the formation of intermittent air fingering surrounded by liquid striations, see Figure 13 for vivid details. These islands of air may shrink, break up into smaller zones, or diffuse within the lubricant. The size and concentration of the ingested air fingers depend on the journal whirl frequency and amplitude and the flow rate. The fluid at the damper discharge is cloudy and foamy, as per Ref. [22] (2001) and Ref. [8] (2003).

The dynamic pressures from air entrainment, Figure 12(b), show important distinctions when compared to those pressures induced by lubricant vapor cavitation, Figure 12(a). In the case of air ingestion, the film pressures differ markedly from one period to the next, the peak pressures show large variations and with pressure spikes as bubbles collapse. Furthermore, the pressure flat zone is nearly at ambient pressure. Note that subambient film pressures occasionally appear. Later, this document presents pressure profiles recorded in SFDs with end seals.

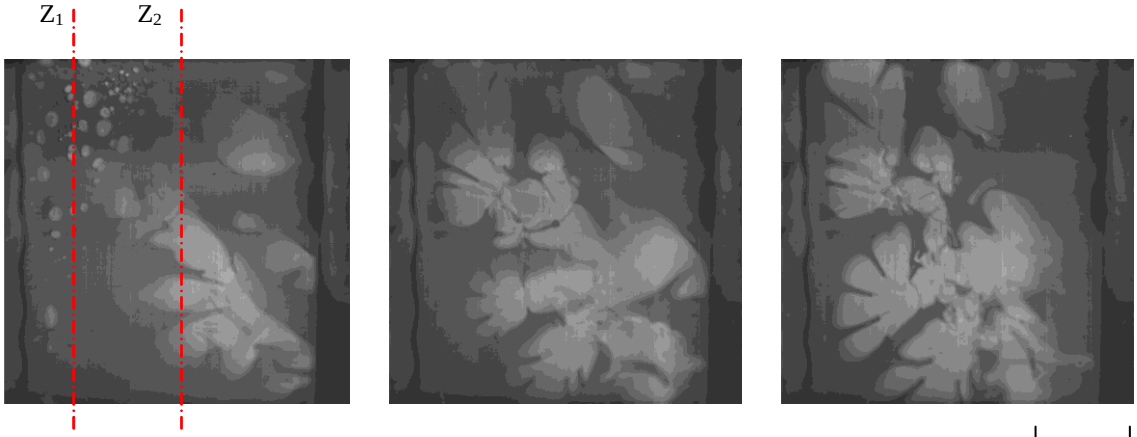

(a) t = 0.026 s
P = 3 kPa at Z_2
h = 140μm

(b) t = 0.028 s
P = 30 kPa at Z_2
h = 270μm

(c) t = 0.030 s
P = 50 kPa at Z_2
h = 380μm

Fig. 13 Photographs of SFD flow field with air ingestion and entrapment. Tests with whirl frequency at 25 Hz and feed pressure 1.93 bar. Elapsed time for photographs is 2 ms (Period = 40 ms). Taken from Ref. [8] (20023).

Inevitably, the vast majority of SFDs operate with foam-like fluids (bubbly mixtures) considering the low magnitude of pressure supply (small through flow rate), large damper clearances, and high operating whirl frequencies. Of course, mixed operation regimes can also occur in practice. For instance, tightly sealed dampers may show both vapor and air entrainment type cavitation where gas bubbles may coexist around a large lubricant vapor bubble. Note that the entrapment of air delays the increase of film pressures since there is less liquid lubricant filling the damper film clearance. Ultimately, operation at high frequencies leads to an increase in air ingestion, preventing any further oil vapor cavitation, and reducing considerably the forces available from the SFD.

Meticulous experimentation demonstrates that air ingestion and entrapment degrades the forced response of open ends SFDs, see Refs. [22] (1999) and [8] (2003). A simple criterion gives the likelihood of air ingestion. The feed-squeeze flow parameter (γ) relates the lubricant supply flow rate Q_{oil} to the dynamic change in volume within the squeeze film gap, i.e.

$$\gamma = Q_{oil}/(\pi L D V_t) \tag{11}$$

where $V_t=(r\omega)$ is the squeeze velocity. When $\gamma>1$ no air entrainment occurs, i.e., the through flow is sufficient to fill the volume change caused by the journal circular whirl motion. On the other hand, air ingestion and entrapment will occur when $\gamma<1$. The lower the feed-squeeze parameter (γ), the more severe the degradation in damper forces. The experimental results advance an empirical correlation between γ and the amount of air entrained (volume concentration of air) in the lubricant, thus providing certainty in the modeling of the mixture. Note that Q_{oil} is proportional to the difference between lubricant supply pressure and discharge pressure and to the flow conductances in the film lands and through the feed ports. The flow conductances (~1/resistances) are a function of the damper clearance and feed characteristics, lubricant and mixture viscosities, etc. Thus, air entrainment is device dependent, and its severity increases with the amplitude and frequency of journal motion; that is, V_t is the fundamental variable. Air ingestion can be prevented by increasing the lubricant supply pressure to ensure a sufficiently large through lubricant flow. This is an impractical recommendation for aircraft engines where weight and oil storage volume are at a premium.

A modern predictive model for SFDs

San Andrés and Koo [10] (2020) extend the original development in [8] (2003) to model dampers sealed with piston rings (PR) and operating with a homogenous bubbly mixture of air in oil. This mixture represents the mixing of entrained gas (air) with the liquid (oil). The air is drawn into the film through regions of low pressure, either ends open to ambient air or through the slits of a PR, for example. The governing equation for the generation of squeeze film pressure (P) is:

$$\frac{\partial}{R\partial\Theta}\left(\frac{\rho h^3}{12\mu}\frac{\partial P}{R\partial\Theta}\right)+\frac{\partial}{\partial z}\left(\frac{\rho h^3}{12\mu}\frac{\partial P}{\partial z}\right)=\frac{\partial}{\partial t}(\rho h)+\frac{\rho h^2}{12\mu}\frac{\partial^2}{\partial t^2}(\rho h) \tag{12}$$

The mixture density ρ_m and viscosity μ_m, depend on the local gas (air) volume fraction (GVF) β,

$$\rho_m = \rho_g + (1-\beta)\,\rho_{oil} \sim \alpha\ \rho_{oil}\ ;\ \mu_m = \mu_g + (1-\beta)\,\mu_{oil} \sim \alpha\ \mu_{oil} \tag{13}$$

with $\alpha=(1-\beta)$ as the liquid volume fraction (LVF). The approximate expressions on the right side of Eq. (13) follow since $\mu_{oil} > \mu_g$ and $\rho_{oil} >> \rho_g$. The GVF (β) depends on the pressure (P) as,

$$\beta_{(P)} = 1-\alpha_{(P)} = \frac{1}{1+\dfrac{P_{(\Theta,z,t)}-P_v}{P_s-P_v}\left(\dfrac{1-\beta_s}{\beta_s}\right)} \tag{14}$$

where β_s is a measured or known at the supply pressure P_s, and P_v ~1 kPa is the lubricant vapor pressure. The model relies on a known state (β_s,P_s). There are more advanced models that include a transport equation for the GVF; see Refs. [23] (2016) and [11] (2023) for example.

In Ref. [10] (2020), physically correct equations for the inlet and outlet flows of lubricant are introduced. Through a feedhole with diameter ϕ_{in} and located at $\{\Theta_{in}, z=z^*\}$ the delivered mass flow of lubricant is

$$\dot{M}_{in} = (\rho Q)_{in} = C_d\left(\tfrac{1}{4}\pi\phi_{in}^2\right)\sqrt{2\rho_{in}\left(P_s - P_{(\Theta_{in},z^*,t)}\right)} \tag{15}$$

where C_d is an empirical loss coefficient. The equation above applies only when $P_s > P_{film}$; otherwise $M_{in}=0$. This condition simulates the operation of a typical mechanical check-valve.

Conventional analyses typically model the outflow through end seals as proportional to a local pressure drop (P_{out}-P_a) and an (empirical) end seal coefficient, see Refs. [14] (1987) and [12] (2022). The overly simplistic model does not apply to a piston ring

as the experimental record shows a jet-like outflow through the PR slits, see Refs. [24,25] (2019) and [26] (2021). As shown in Fig. 16, the mass flow through a PR slit with area A_{slit} is

$$M_{exit} = C_{slit} A_{slit} \sqrt{2\rho \left| P_{\left(\theta_{slit}, \frac{L}{2}, t\right)} - P_a \right|} \tag{16}$$

The Eq. above allows for both the outlet flow and inlet flow of a mixture through the PR slit opening.

In the model, the greatest unknown relates to the quantification of the gas volume fraction (β), an outcome of the squeeze film kinematics and end seal conditions. Rodriguiez and San Andrés in Ref. [27] (2024) resolved this last hurdle in a surprisingly simple way. A procedure draws a sample of the bubbly fluid into a balloon; and by measuring the volume and weight of the inflated balloon produces an accurate estimation of the ingested GVF. Recent video graphic evidence of air ingestion and entrapment along with recorded dynamic pressures in the squeeze film land will be detailed after presentation of a test rig and the procedure for identification of force coefficients.

Description of a modern SFD test rig and parameter identification procedure

Dedicated test rigs to measure squeeze film pressures and SFD journal motions due to imposed dynamic loads are described in the literature; see Refs. [16] (1985), [4] (1996), [20] (1997), [8] (2003), and [19] (2010) for early test rigs at Texas A&M University.

Presently, the discussion focuses on a test rig constructed with funding from a major aircraft engine company and whose major aim is to quantify the performance of ultra-short length SFDs with end seals. The configurations are directly applicable to aircraft engines. Refs[4]. [6] (2016), [24,25] (2019), [26] (2021), [27] (2024) detail the measurements and parameter identification, the identified force coefficients from small and large amplitude whirl motions over a wide frequency range, and comparisons to physical model predictions.

Figure 14 depicts the SFD test rig comprising a rigid pedestal, four support rods, a journal, and a bearing cartridge (BC). Two orthogonally placed electromagnetic shakers and stingers apply dynamic loads to the BC and produce circular or elliptic orbites, centered of off-center. Installed in the BC, along the X and Y axes, pairs of accelerometers, eddy current sensors, and load cells measure the BC accelerations, the displacements relative to the fixed journal, and the applied shaker loads. Figure 15 shows top and cross-section views of the BC and journal with end grooves for installation of O-rings. The squeeze film section is short in axial length, L = 25.4 mm, and the journal diameter D = 127 mm (L/D=0.2). The film radial clearance c = 0.373 mm, although dampers with other various clearances were constructed.

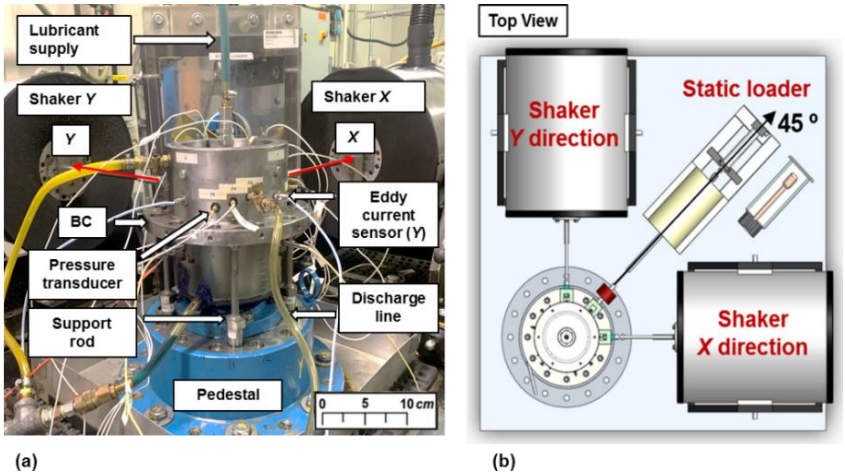

Fig. 14 (a) Photograph and (b) schematic top view of SFD test rig with electromagnetic shakers and static loader.

4 The research program produced over 30 journal papers and a greater number of conference papers. Please visit http://rotorlab.tamu.edu for a full list of publications.

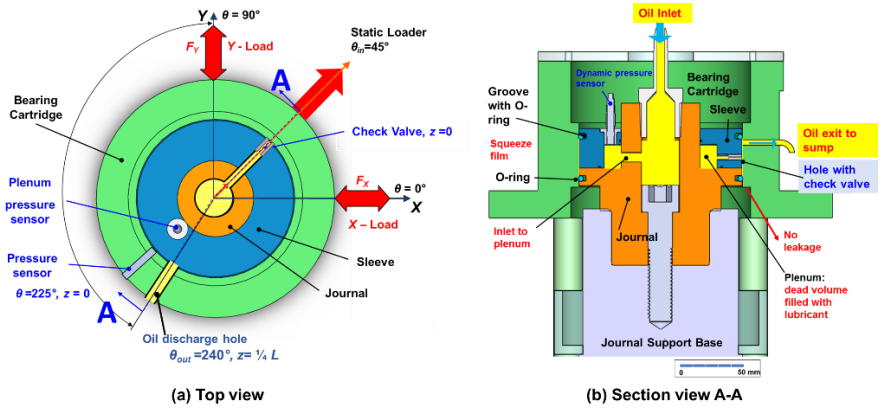

Fig. 15. OR-SFD (a) top view featuring one lubricant feedhole (θ_{in} = 45º, z = 0) and a discharge hole (θ_{out} = 240º, z = +¼ L); and (b) section A-A showing installed ORs. (Drawings not to scale and with exaggerated features). From Ref. [26].

A pump supplies ISO VG 2 lubricant at pressure P_S ranging from low=0.69 bar(g) to high=6.9 bar(g). At a feed temperature of 25 ºC, the lubricant viscosity is $\mu = 2.81 \pm 0.01$ mPa-s and its density $\rho = 800 \pm 0.02$ kg/m^3. The viscosity quoted is like that in an aircraft jet engine (~ 200 ºC). Oil flows through a check valve and orifice into the middle plane of the film land (z=0). The journal has end grooves at z= +/- ½ L for installation of end seals, either O-rings (OR), or piston rings (PR), or open to ambient (no end seals).

Orings are very effective end seals since their offer a large flow resistance, practically null flow. In an OR-SFD configuration, the oil exits through one discharge orifice at z= + ¼ L that connects to a return line. A return pump pushes the lubricant through a bubble eliminator and into a storage tank. In a PR-SFD configuration, as shown in Fig. 16, the lubricant leaves the damper through the slits of the top and bottom piston rings.

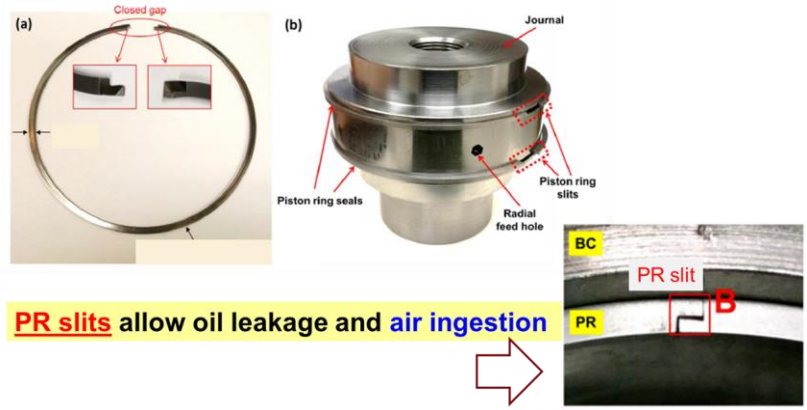

Fig. 16. SFD journal and installed piston rings.

The experiments comprise single-frequency dynamic loads over a frequency range ω=10 to 130 Hz, in increments of 10 Hz. The test rig is idealized as a two degree of freedom (DOF) mechanical system with the cartridge mass (M_{BC}) attached to the elastic support structure, the O-rings or PRs, and the squeeze film section. Fig. 17 showcases the idealized mechanical system and its fundamental elements; namely, stiffness (K), damping (C), and inertia (M) coefficients.

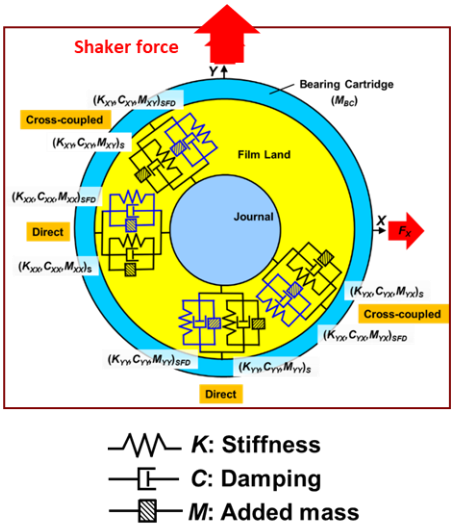

Fig. 17. Schematic view of SFD test rig as 2 DOF system.

Under lubricated conditions, the equation of motion in the frequency domain [28] is

$$\mathbf{H}_{L_{(\omega)}}\mathbf{Z}_{(\omega)} = \mathbf{F}_{(\omega)} - M_{BC}\,\mathbf{a}_{(\omega)} \tag{17}$$

where M_{BC}=15.6 kg is the bearing cartridge mass, and $\mathbf{F}_{(\omega)}$, $\mathbf{Z}_{(\omega)}$ and $\mathbf{a}_{(\omega)}$ are complex vectors for the applied force, BC displacement relative to the journal, and BC absolute acceleration, respectively. Above, $\mathbf{H}_L$ is a 2x2 matrix representing the lubricated system complex dynamic stiffness, and which includes the physical parameters from the structure, ORs or PRs, and the squeeze film. For the OR-SFD, let

$$\mathbf{H}_L = \mathbf{H}_{st+OR} + \mathbf{H}_{SFD} \tag{18}$$

where

$$\mathbf{H}_{st+OR} = \mathbf{H}_{st} + \mathbf{H}_{OR} = \begin{cases} \mathbf{H}_{st} = \left[\mathbf{K}_{st} - \omega^2\mathbf{M}_{st}\right] + i\,\omega\,\mathbf{C}_{st} \\ \mathbf{H}_{OR} = \mathbf{K}_{OR} + i\,[\omega\mathbf{C}_{OR} + \mathbf{K}_{\perp}] \end{cases} \tag{19}$$

Above, the support structure has stiffness, damping and mass $(\mathbf{K, C, M})_{st}$. The O-rings dynamic forced response is modeled with a viscous damping coefficient ($\mathbf{C}_{OR}$), a restoring stiffness ($\mathbf{K}_{OR}$), and a quadrature stiffness ($\mathbf{K}_{\perp}$). Without the O-rings installed and no lubricant in the system, first measurements produce the support ($\mathbf{H}_{st}$), and curve fits over a frequency range deliver the physical parameters $(\mathbf{K, C, M})_{st.}$

Next, the ORs are installed in the journal and still with a dry (no oil) structure, a new set of dynamic loads produces $\mathbf{H}_{st+OR,}$ the parameters of the ORs plus the structure. Then, $\mathbf{H}_{OR} = [\,\mathbf{H}_{st+OR} - \mathbf{H}_{st}]$.

Lastly, lubricant is supplied into the damper at a set pressure (P_S), and a new round of dynamic load tests performed to obtain the complex dynamic stiffness $\mathbf{H}_L$ of the lubricated system. The squeeze film parameters follow from $\mathbf{H}_{SFD} = \mathbf{H}_L - \mathbf{H}_{st+OR}$.

Curve fits over a certain frequency range produce the SFD stiffness, damping and added mass coefficients from

$$\mathbf{H}_{SFD} = \left[\mathbf{H}_L - \mathbf{H}_{st+OR}\right] \rightarrow \left[\mathbf{K}_{SFD} - \omega^2\mathbf{M}_{SFD}\right] + i\,\omega\,\mathbf{C}_{SFD} \tag{20}$$

The procedure identifying the parameters of a SFD sealed with piston rings is identical.

Effect of supply pressure on SFD force coefficients

For centered whirl orbits with amplitude e/c = 0.3, Fig. 18 presents the experimental SFD direct damping C= ½ (C_{XX}+C_{YY}) and added mass M= ½ (M_{XX}+M_{YY}) coefficients for the two test dampers as the oil supply pressure (P_S) increases. During the tests, the maximum squeeze film speed = 70 mm/s and the largest squeeze Reynolds #, Re_s~26. For the PR-SFD, C increases 30% as P_S grows from 2.1 bar to 6.2 bar whereas M remains nearly constant at ~30 kg. For the OR-SFD, C increases ~11% as P_S increases whereas M decreases ~13%. The added mass (M) for the OR-SFD is 16% larger than that of the PR-SFD. In short, for P_S > 2 bar the OR-SFD produces slightly ~ 11 % more damping than the PR-SFD does since the O-rings provide a perfect seal (no leakage). The PRs allow for leakage through its slits (abutted ends). Note that the damping discussed above is only the viscous portion. The OR-SFD produces ~10% more damping with the addition of the damping coming from the viscoelasticity of the O-rings; see Refs.

[24] (2019), [25] (2021), and [26] (2024) for details on the identified OR force coefficients.

The graphs include predictions based on Eq. (9) for a SFD without any side leakage, i.e., fully sealed. C_*=12.8 kNs/m ad M_*=44 kg. Note the experimental C approaches the theoretical magnitude as the supply pressure increases. The added mass coefficient is ~ 60% of the prediction but still having a large magnitude, nearly twice the mass of the bearing cartridge (M_{BC}).

Note the experimental force coefficients are different from the ideal predictions based on Eq. (9) because the test dampers have feed holes acting as sources of constant pressure and means of evacuating the lubricant through either the slits of the piston rings or an exhaust orifice in the OR-SFD. The PR-slits and exit hole act as (local) sinks of flow. Both inlet and exit conditions contribute to distort the squeeze film pressure field making it markedly different from the idealized one.

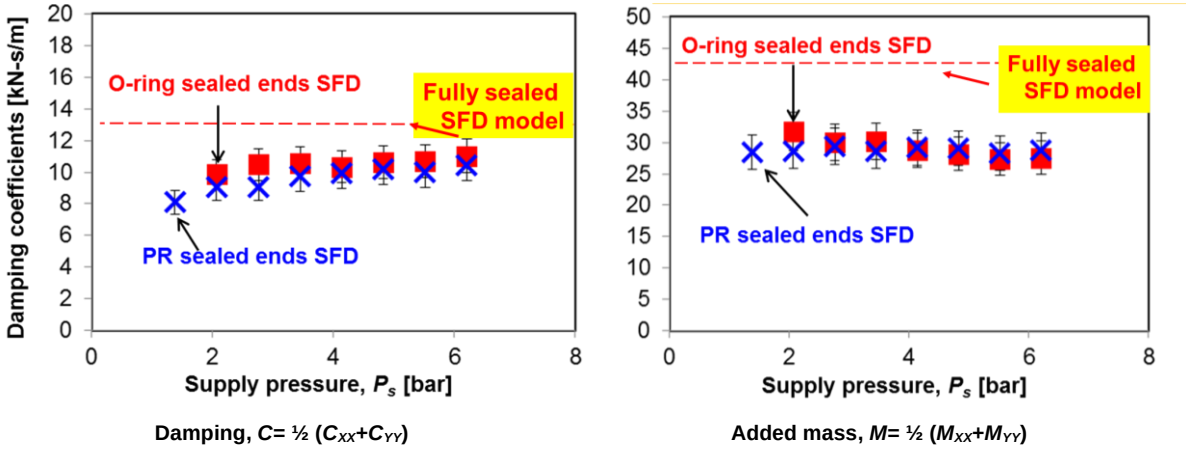

Fig. 18 OR-SFD vs. PR-SFD: direct damping (C) and added mass (M) coefficients vs. lubricant supply pressure (gauge). Circular centered orbits with amplitude e/c = 0.3 and whirl frequencies 10- 100 Hz. (Three feedholes)

Effect of static eccentricity and orbit amplitude on SFD force coefficients

Figure 19 shows the experimental damping (C_{XX}, C_{YY}) and added mass (M_{XX}, M_{YY}) coefficients for both dampers supplied with a low supply pressure. In the graphs, the horizontal axis denotes the orbit amplitude (e/c) and data corresponds to two static eccentricities, e_s = centered and 0.3c. The results are presented in dimensionless form as $\underline{C}=C/C_*$ and $\underline{M}=M/M_*$. Note that $\underline{C}$ and $\underline{M}$ of order one (~1.0) denote perfect correlation with the theoretical prediction for a fully sealed SFD. The predictions are derived from the orbit model in Ref. [7] (2016) that reproduces the kinematics of the journal.

Note the journal static eccentricity has a small effect on both force coefficients for the PR-SFD. The OR-SFD shows more damping for the off-centered condition (e_s =0.3c). In general, the OR-SFD damping and added mass coefficients increase by ~30% and 20% as the orbit amplitude of motion increases. Note the PR-SFD is less sensitive to changes in both orbit amplitude and off-centered condition. The model predictions are in good agreement with the test data.

Effect of number of (open) feedholes on SFD force coefficients

It is of great interest to quantify the performance of SFDs when one or more feedholes clog, hence blocking the passage of fresh lubricant into the film land region. A mechanical check valve could also fail and stop the oil flow. Fig. 20 shows the experimental damping ($\underline{C}_{XX}$, $\underline{C}_{YY}$) and added mass ($\underline{M}_{XX}$, $\underline{M}_{YY}$) coefficients for both dampers vs. orbit amplitude. Supplied with oil at 0.69 bar(g), the dampers operate with either three feedholes or one feedhole (two holes blocked). In short, having one-feedhole generates more damping and added mass coefficients. The finding appears contradictory to common sense; however, note that feedholes are source of constant pressure and locally distort the pressure field, hence preventing the generation of squeeze film pressure. Note that one or three feed holes make a large difference on the performance of the OR-SFD. The PR-SFD with one feed hole produces less damping that the OR-SFD does, but its added mass coefficient is larger. The OR-SFD with one open feedhole produces 60% more damping than the configuration with three holes. For the dampers with one feedhole, $C_{\text{PR-SFD}} < C_{\text{OR-SFD}}$ and $M_{\text{PR-SFD}} < M_{\text{OR-SFD}}$ due to air ingestion thru the PR slits.

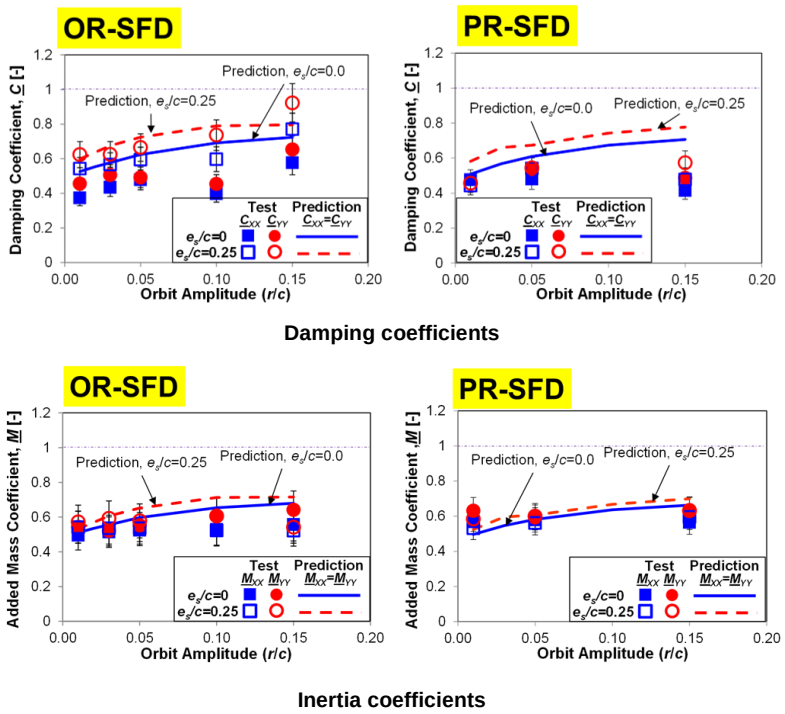

Fig. 19 OR-SFD vs. PR-SFD: dimensionless direct damping (*C*) and added mass (*M*) coefficients vs. orbit amplitude and two static positions. Oil supply pressure 0.69 bar(g). Three open feedholes. Taken from Ref. [24] (2019).

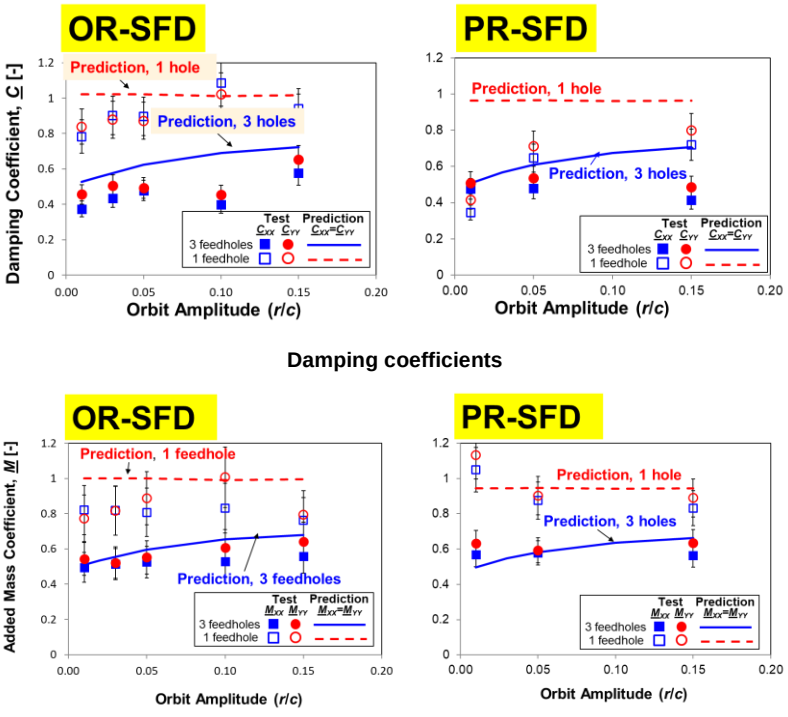

Fig. 20 OR-SFD vs. PR-SFD: Three and one feedholes. Dimensionless direct damping (*C*) and added mass (*M*) coefficients vs. orbit amplitude. Static eccentricity=0 an oil supply pressure 0.69 bar(g). Taken from Ref. [24] (2019).

The orbit-model predictions for the three-hole dampers are good. The agreement is lesser for the one-hole dampers that particularly overestimate the damping coefficient. The model underestimates the influence of air ingestion and entrapment. Although the dampers' ends are sealed, the experimental force coefficients are ~50% of the theoretical fully sealed model, see Eqs. (9), on account of the low magnitude of the oil supply pressure.

Examples of pressure profiles and photographs of oil condition

The decades long research program strived to build dedicated test SFD rigs and measurement procedures to identify the dynamic forced response of SFDs. A fundamental aspect of the research is the measurement of the dynamic pressure waves in the film land of a test damper. Detailed pressure measurements and interpretation of phenomena can be found in Refs. [16] (1985), [20] (1997), [22] (1999), [8] (2003), [6] (2016), [24] (2019), [10] 2020, [24,25,26] (2019), [11] (2023), and [27] (2024). The discussion centers on ascertaining the relevance of oil vapor cavitation, gas oil cavitation and air ingestion and entrapment.

As relevant example, Fig. 21 displays graphs for three periods of pressure waves recorded at the midplane of a PR-SFD and at two angular locations, 225º and 315º. For reference, the oil supply pressure (P_S) increases from low (top graph) to high (bottom graph). The damper describes circular centered orbits with amplitude e=0.65 c at a frequency of ω=60 Hz; hence, $V_t = e\omega$ =60 mm/s. For the same P_S, note the significant differences in film pressure waves at the two angular locations although the journal kinematics process is identical. Both peak-peak pressures differ, and they are not out of phase by 90º as the journal motion would dictate for an idealized damper (no holes or sinks). That is, the location of the feedhole and the PR slits affects the pressure waves. Note that the magnitude, peak-peak, of the film pressures increases as the supply pressure increases. At the lowest P_S =0.69 bar(g), oil vapor cavitation appears, and air ingestion is small since film pressures are also small. At the intermediate pressure P_s=2.8 bar(g), the film peak-to-peak pressures are larger, and with a persistent air ingestion, produce noisy pressure waves with sudden pressure bursts (high frequency) that make the gas bubbles collapse. The highest P_S =6.9 bar(g) is large enough to prevent either air ingestion or lubricant vaporization. Hence, as shown in the prior figures, the PR-SFD will produce force coefficients increasing in magnitude as the supply pressure P_S grows from lowest to highest.

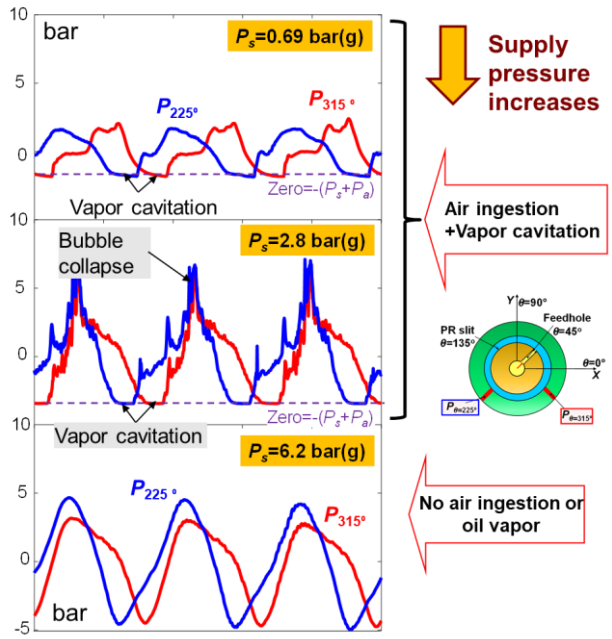

Fig. 21 PR-SFD: Measured dynamic film pressure waves at two angular locations vs. magnitude of oil supply pressure,0.69 to 6.2 bar(g). Circular centered orbits with amplitude e=0.65 c and frequency 60 Hz. One feedhole. Squeeze film speed V_t = 90 mm/s and squeeze film Reynolds # Re_s= 15.52. Taken from Ref. [24] (2019).

Figure 22 shows photographs of the oil exiting the PR-SFD for two oil supply pressures. The journal kinematics are the same as those in Fig. 21. For the low P_S, the oil bubbles through the PR slit to make a foamy mixture. For the high P_S, liquid jets out through the PR slit and the lubricant accumulating on the exit side shows less bubble. The higher supplied flow rate (at the higher P_S) prevents the ingestion of air into the squeeze film, as shown in Fig. 21 (bottom graph).

Similarly, Figure 23 depicts photographs of the time evolution of the lubricant exiting the PR-SFD and its accumulation on the top side. Note the major differences for operation at two pressures, one low and one moderately high. For the low P_S, there is more air ingestion that, as time progresses, makes a foamy mixture. The photographs show the PR cannot fully seal the lubricant flow as there is persistent leakage through the PR slits.

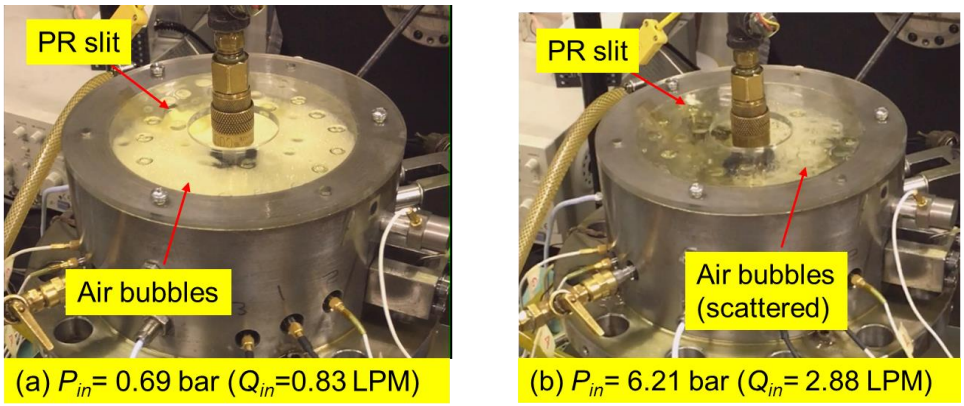

Fig. 22 PR-SFD: Photographs of lubricant exiting on the top side. (a) P_S=0.69 bar(g) (Q_{in}=0.83 LPM) and (b) P_S=6.21 bar(g) (Q_{in}=2.88 LPM). Circular centered orbit with frequency 60 Hz and orbit radius e =0.65c. One lubricant feedhole. Taken from Ref. [24] (2019).

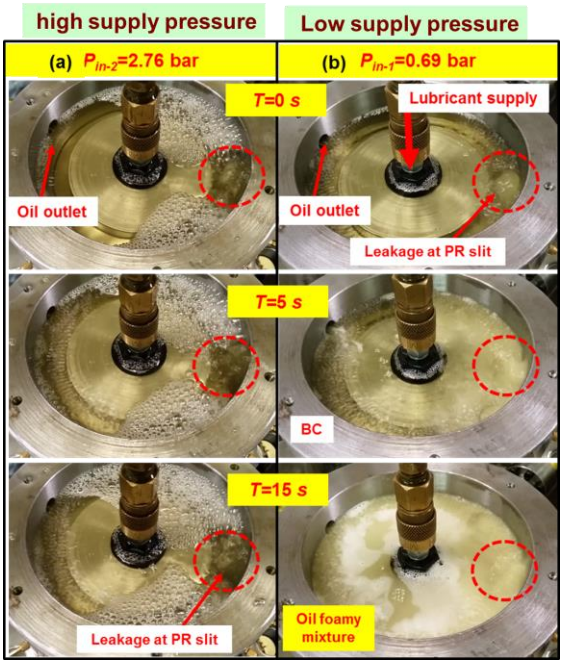

Fig. 23 PR-SFD: Photographs of evolution of lubricant exiting on top side of damper. (a) P_S=2.76 bar(g) and (b) P_S=0.69 bar(g) bar (Q_{in}=2.88 LPM). Taken from Ref. [25] (2019).

Table 2 below shows the URLs for several short videos recorded during the experiments. The videos make palpable the persistence of air ingestion and entrapment on the operation of dampers (open ends, piston rings sealed, or with O-ring seals) and under large enough squeeze film velocities. In general, increasing the lubricant supply pressure to avoid or to ameliorate the detrimental effect of air entrapment in a SFD is not practical for aircraft jet engines. The demand of a high-pressure pump more and larger volume for oil storage are not options in an application where weight and volume are at a premium.

The last video keeps a record of the method to a quick way to quantify the entrained gas volume fraction (GVF) while the damper is in operation. The breakthrough procedure can readily assist the validation of computational models and to predict

accurate force coefficients.

Table 2. Universal record locators (URLs) for video clips of SFD performance and oil exit condition

URL	Short description	Reference
https://www.youtube.com/watch?v=Tqceie9mbdE	SFD test rig overview at Rotordynamics Laboratory	(2020) Texas A&M University
https://www.youtube.com/watch?v=T_MchmIPItk	Jet engine SFD research overview	(2018) Texas A&M University Public Relations Office
http://youtu.be/8wQ1TnGTmyE http://youtu.be/6xNra8umKEw	Open SFD – Condition of lubricant exiting to top side and bottom side. L = 25.4 mm, c = 0.025 mm, P_s = 0.41 bar(g), flow: 5. 0 liter/min	(2014) Texas A&M University
https://www.youtube.com/watch?v=PulQisPDRtY	PR-SFD: Time Evolution of lubricant condition through top exit section. Two supply pressures	Ref. [24] (2019)
https://youtu.be/R5WPD6t1fWs	OR-SFD: Lubricant flow exit condition for increasing squeeze velocities	Ref. [27] (2024)
https://youtu.be/AtVBw5XMdcw	OR-SFD: Measurements to estimate the GVF from experiments with orbit amplitude r = 0.15c to 0.45c and whirl frequency ω = 55 Hz and 70 Hz.	Ref. [27] (2024)

Figure 24 shows the measured GVF vs. squeeze film velocity ($V_t = e\omega$) obtained in a tightly sealed OR-SFD supplied with lubricant at a low pressure, P_s= 0.69 bar(g). During the measurements, the circular centered orbits had amplitudes ranging from e=0.20c to 0.45c, and the whirl frequency reached 70 Hz. Note the GVF, i.e. the amount of air ingested, increases as the squeeze velocity increases above a threshold magnitude ~ 25 mm/s. At the largest V_t =55 mm/s (e=0.45 and w=70 Hz), the amount or air ingested is ~ 58%. At this operating condition, the lubricant leaving the damper through a discharge hole is just a foamy mixture.

One must realize the O-rings are not perfect seals because, while they undergo large orbital motions and frequencies, they relieve their assembly compression pressure and allow for air ingestion, lots of it!

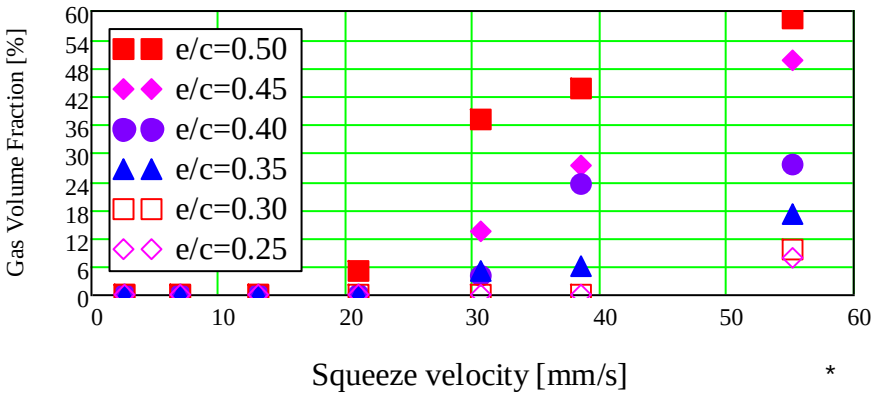

Fig. 24 OR-SFD supplied at 0.69 bar(g): Quantified gas volume fraction (GVF) vs. squeeze velocity (V_t=$e\omega$) and orbit amplitude (e/c). Whirl frequency 70 Hz max. Data in Ref. [27] (2024).

OR-SFD vs PR-SFD – Lessons Learned

(a) The OR-SFD produces more damping as it avoids air ingestion. O-rings add stiffness and viscoelastic damping to a test system.

(b) For both PR-SFD and OR-SFD, the larger the number of active feed holes, the lower the damping coefficient. Holes distort and reduce dynamic pressure field, hence the lesser force coefficients.

(c) Damping for OR-SFD increases with static eccentricity (e_s), whereas added mass for OR-SFD and damping and added

mass for PR-SFD remain nearly constant.

(d) Neither the OR-SFD nor the PR-SFD generated cross-coupled force coefficients. That is, $C_{XY} = C_{YX} = 0$ and $M_{XY} = M_{YX} = 0$

(e) Film pressures show oil vapor cavitation and persistent air ingestion for operation with a lubricant supplied at a low pressure and for journal motions with a large squeeze velocity (V_t).

(f) The amount of air entrained in a sealed damper is a function of the squeeze velocity (> threshold) and the pressure supply. Piston rings leak profusely and ingest lots of air. O-rings may appear as a best sealing option, however they quickly degrade once they lose their compression (squeeze) assembly.

The Integral Squeeze Film Damper

The basic design of SFDs changed little until the middle 1990's when the wire-EDM processes enabled the construction of integral dampers (ISFDs), see Ref. [29] (1995). ISFDs offer distinct advantages such as reduced overall weight and length of the damper structure with lesser number of parts, accuracy of positioning (centering), and a split segment construction allowing easier assembly, inspection and retrofit than with any other type of damper.

Flexure pivot tilting pad bearings offer similar construction features while minimizing (assembly) stack up tolerances and avoiding pivot wear and fretting. These features are most important in aircraft engines where reduced weight and size are an important consideration. The ISFD, shown in Figure 25, comprises of segmented pads instead of a fully cylindrical journal. Thin structured webs attach the inner and outer rings and perform the function of elastic supports. The thin gap between the pads and the outer ring forms the squeeze film lands. Each pad can be manufactured with a different clearance to counter the static deflection due to rotor weight. Side seals, typically end plates with a tight gap, restrict the axial flow through the film lands, and amplify the damping coefficients by rising the dynamic pressure in a lubricated film undergoing squeeze motions.

The series combination of a tilting pad bearing with a squeeze film damper has been implemented in numerous compressors to introduce flexibility and damping to the bearing support. The engineered selection of these two mechanical elements determines the relocation of the (rigid mode) rotor bearing system critical speeds, well below the mean operating speed, along with an optimum damping coefficient at the bearing support. The low structural stiffness of a ISFD and its damping also isolate the rotor-bearing system from its casing and foundation.

Ref. [30] (1999) is the first to present an experimental verification of the damping capability of a sealed ISFD. The tighter the clearance of the end plate seals, the larger the ISFD damping coefficient. Later in 2003, Ref. [31] presents imbalance response measurements of a rotor supported on flexure pivot bearings in series with ISFDs. The mechanical element is often referred as a damper bearing. The experimental results confirmed the lubricated bearing-ISFD single element, short in axial length as shown in Fig. 25, accurately controlled the location of the test system critical speed and certified the predicted amplification factor for the rotor response.

Despite the commercial applications of ISFDs[5], the identification of force coefficients for ISFDs has not seen many concerted efforts. Delgado et al. [32] (2011) and Agnew and Childs [33] (2012) test a flexure pivot bearing in series with an ISFD. In Ref. [32], Delgado et al. find the ISFD generates a significant added mass, until largely ignored by manufacturers specifications. Similarly, Agnew and Childs [33] report the series mechanical element (active ISFD) produces small stiffnesses and damping coefficients, ~ 50% or more of the force coefficients for the hydrodynamic bearing alone (locked ISFD). The reduction in K, C as rotor speed increases is the expected outcome. Ref. [33] also reports added mass coefficients ~ 20 kg for the damper bearing and 20 to 40 kg for the flexure pivot bearing alone. Contrary to a common assumption, the series bearing-ISFD produces less damping, not more.

Recently, dedicated test campaigns have produced force coefficients (K, C, M) for ISFDs with the intention of further their adoption in upcoming high-speed, compact turbomachinery processing CO_2 for carbon capture and sequestration, and in waste heat generation. See Refs. [34] (2018) and [35] (2021).

Figure 26 depicts the test ISFD in Ref. [35]. The damper axial length L=76 mm, film clearance c=0.356 mm, and four 73º circular pads at a diameter of D=157 mm. Conducted in the test rig described in Ref. [33], the experimental work quantified the ISFD force coefficients as a function of the static eccentricity (load) and the gap ($b_{1`}$) configured in the end plate seals. The pseudo random generated dynamic loads had an excitation frequency ranging from 9 to 166 H and produced bearing motions of small amplitude (relative to the clearance). For reference the elastic structure stiffness K_S ~ 60 MN/m, and the mass of the housing and ISFD M_{BC} = 19 kg. At 46ºC, the supplied ISO VG46 oil viscosity and density equal μ=32 cPoise and ρ=860 kg/m^3, respectively.

[5] Suggestion: watch the video clip from an ISFD fabricant: **https://www.youtube.com/watch?v=HlXZNQYFbXk**

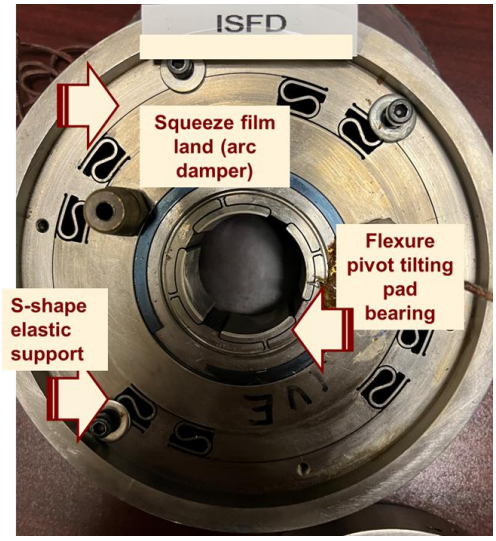

Fig. 25. Series integral SFD and flexure pivot tilting pad bearing.

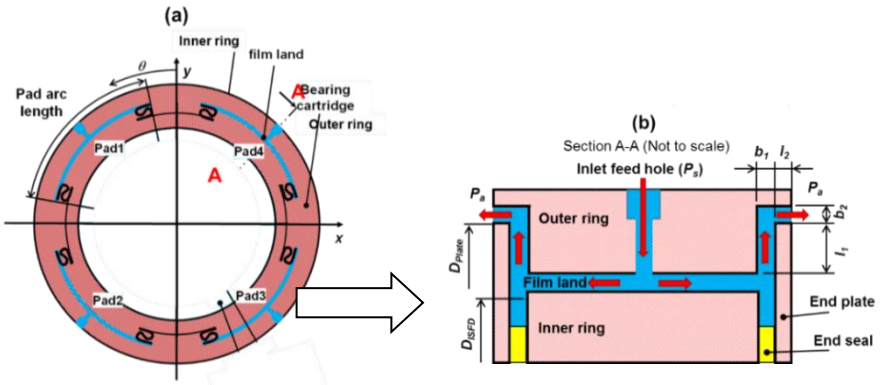

Fig. 26 Test ISFD front view and cross section showing lubricant flow path (not to scale).

Figures 27 and 28 display the test ISFD damping (C_{XX}, C_{YY}) and added mass (M_{XX}, M_{YY}) coefficients vs. static eccentricity (e_s) and for several end seal gaps, b_1. The parameters shown are *true* rotordynamic coefficients since they correspond to small amplitude motions around e_s. At the largest e_s=0.7 c, the applied static load (toward a pad center) equals 14.95 kN. The tightest end seal gap of 0.28 mm, b_1/c = 0.78, severely restricts the axial flow and the ISFD generates quite large damping coefficients, approximately 22 times more than the coefficient estimated for the open ends ISFD. Similarly, the added mass coefficients are large, ~50 kg for the ISFD with end seal gap of 0.53 mm, b_1/c = 1.5.

Note both damping and inertia coefficients grow modestly as e_s increases. On the other hand, predictions shown in Ref. [35] are highly nonlinear, albeit agreeing with the experimental results for the smallest e_s. Worthy of note, the tests with the tightest end seal (b_1/c = 0.78) produced an unexpected stiffening of the test bearing, i.e., a negative added mass. The unusual effect is due to the compressibility of the lubricant having a small amount of dissolved gas. In a ISFD with very tight end seals, the lubricant cannot easily displace either axially or circumferentially, hence the squeeze film action generates a dynamic pressure field that compresses the fluid to produce the hardening effect.

Simple formulas for estimating the damping (C) and added mass (M) of ISFDs are:

$$C_{ISFD\_open} := \left(\frac{Pad_{arc}}{90}\right)\cdot\pi\cdot\mu\cdot\frac{D}{2}\cdot\frac{L^3}{c^3} \qquad C_{ISFD\_sealed} := \left(\frac{Pad_{arc}}{90}\right)^3\cdot\frac{12}{8}\cdot\pi\cdot\mu\cdot\frac{L\cdot D^3}{c^3}$$

$$M_{ISFD\_open} := \left(\frac{Pad_{arc}}{90}\right)\cdot\pi\cdot\rho\cdot\frac{1}{24}\cdot\frac{D\cdot L^3}{c} \qquad M_{ISFD\_sealed} := \left(\frac{Pad_{arc}}{90}\right)^3\cdot\frac{1}{8}\pi\cdot\rho\cdot\frac{L\cdot D^3}{c} \tag{21}$$

Above, the pad arc is in degrees. The formulas, applicable to motions around the journal centered position, were derived first published in Ref. [30] (1999) to model ideal open ends ISFD and fully sealed (no leakage) ISFD. The equations do not account for feed holes or the end seals flow resistance. Please see Ref. [35] (2021) for details on an accurate finite element computational model that includes fluid compressibility. Note the ratio of force coefficients sealed/open ends = 3 (D/L x $Pad_{arc}/90)^2$.

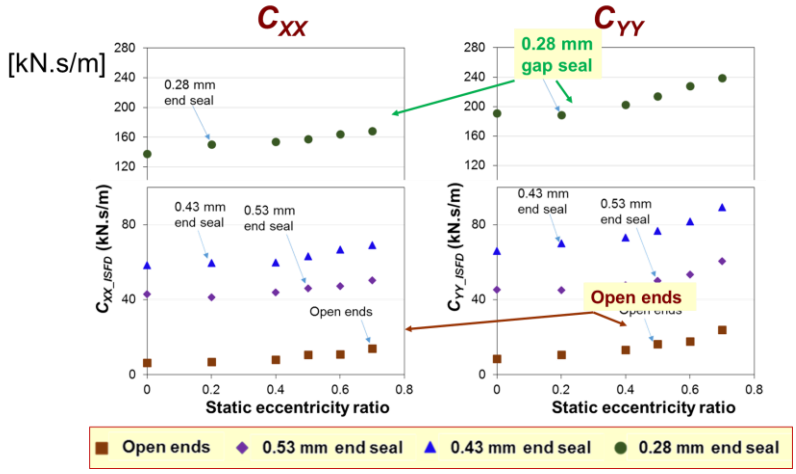

Fig. 27 ISFD experimental damping coefficients vs. static eccentricity and several gaps in the end seals. Clearance *c*=0.356 mm. Taken from Ref. [35].

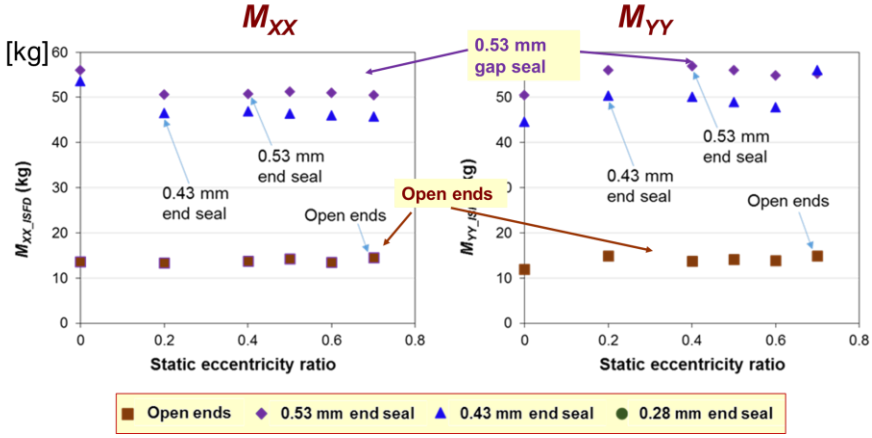

Fig. 28 ISFD experimental added mass coefficients vs. static eccentricity and several gaps in the end seals. Clearance *c*=0.356 mm. Taken from Ref. [35].

The learning to date

Decades of practice demonstrate that squeeze film dampers generate damping even when operating with persistent air entrainment. Dampers also produce significant added mass coefficients, often larger than the journal mass. The structural stiffness soft of the damper support (squirrel cage or flexures) is the key parameter that allows the device to displace and generate a reaction force. That is, dampers must *see* journal dynamic displacements to produce a dissipation force. Due to persistent air

ingestion, the damping coefficient decreases for operation with large squeeze film velocities (amplitude of motion x whirl frequency). The reduction in damping at high frequencies and large amplitudes is beneficial in rotor-bearing systems operating away from critical speeds.

Last millennium, Childs (3) [1993] noted that because of lubricant cavitation and unquantifiable air ingestion, correlation between theory and experiment is less compelling for SFDs than for journal bearings. Presently, Childs' assertion does not hold since state-of-the-art predictive models, accounting for fluid inertia, feed grooves and holes, and air ingestion and entrapment, produce damper forces in agreement with the experimental record. Overly simplistic models based on classical lubrication continue to do poorly. The idealized geometry models predict damper force coefficients which are highly nonlinear, varying greatly with the static eccentricity or the orbit amplitude. The experimental record demonstrates that SFDs and ISFDs are quite linear mechanical elements; that is, both the motion amplitude and static off-centering influence little the magnitude of the damping and inertia force coefficients.

In the design of stable rotordynamic systems, damping is the critical design consideration. If damping is too large, a SFD acts as a rigid constraint to the rotor-bearing system with large forces transmitted to the support structure. If damping is too light, the damper is ineffective and would permit excessively large amplitudes of rotor motion, often subsynchronous. In actuality, the physical magnitude of the damping coefficient is irrelevant; rather the viscous damping ratio for the whole system is important. Hence, SFDs are to be designed and implemented with full knowledge of the rotor-bearing system, namely modal stiffnesses and masses that define the system natural frequencies and the modal damping ratios. Hence, to be effective, a damping element must be "soft" to allow for motions (or displacements) at the location of the support when crossing natural vibratory modes (traversing critical speeds). As a cautionary note, dampers designed with overly tight end seals could produce damper lock-up due to their sizeable viscous damping and stiffness hardening. The lubricant, confined into a fixed volume, has no route for ready evacuation.

Although ISFDs have been around for ~ 30 years, their application is still limited to certain types of centrifugal compressors; often in the aftermarket as a drop-in retrofit. Their major role is to displace system critical speeds away from the mean operating speed. In this last case, ISFDs offer also structural isolation. Despite their significant advantages, the use of ISFDs in aircraft engines has not taken place. Their time is ripe, as air breathing engine manufacturers search for ultra-short damper configurations (L/D~0.2), five to seven in a typical engine. The savings in axial space will shorten overly long, multiple shaft flexible rotors. Combined flexure-pivot hydrodynamic bearings in series with ISFDs are quite promising for the novel application of Carbon capture and sequestration & waste heat generation as well as the upcoming Hydrogen processing turbomachinery.

Nomenclature

(A_X, A_Y)	Components of journal acceleration [m/s^2]
a_r	$-e\omega^2$. Journal radial acceleration
b_1	End plate seal axial gap [m]
c	Film land clearance [m]
$C, C_{\alpha\beta}$	Damping coefficients, $_{X,Y}$ & r,t [N.s/m]
D	$D = 2R$. Journal diameter [m]
e_s	Journal static eccentricity [m]
e	Journal orbit radius (r) [m]
ε	e_s/c. Static eccentricity ratio [-]
(e_X, e_Y)	Components of journal center displacement [m]
(F_X, F_Y)	Components of SFD reaction force [N]
h	Film thickness [m]
$H_{\alpha\beta}$	System complex dynamic stiffnesses [N/m]
i	Imaginary unit
$K, K_{\alpha\beta}$	Static stiffnesses, $_{\alpha\beta=X,Y}$ & r,t [N/m]
K_s	Bearing structure static stiffness [N/m]
L	Damper axial length [mm]
$M, M_{\alpha\beta}$	Added mass coefficient, $_{\alpha\beta=X,Y}$ & r,t [kg]
M_{BC}	Mass of bearing and support structure [kg]
M_o	($\rho\, \pi\, DLc$). Mass of fluid in squeeze film [kg]
M_J	($\frac{1}{4}\, \rho_{steel} \pi D^2 L$). Mass of steel journal [kg]
P	Pressure field [Pa]
P_S, P_a	Oil supply pressure and ambient pressure [Pa]
Q_{oil}	Suplied lubricant flow {m^3/s)
(r,t)	Radial and tangential coordinates.
Re_s	$(\rho/\mu)\omega c^2$. Squeeze film Reynolds number
(V_X, V_Y)	Components of journal center velocity [m/s^2]
V_t, v_s	$e\omega$. Tangential velocity or squeeze film velocity [m/s]
(X,Y)	Coordinate system on plane of bearing [m]
z	Axial coordinate [m]
β	Gas volume fraction [-]
γ	$Q_{oil}/(\pi\, L\, D\, V_t)$. Squeeze-flow parameter (open ends SFD)
μ	Oil viscosity [Pa.s]
ρ	Oil density [kg/m^3]
θ	circumferential coordinate [-]
ω	Excitation frequency [rad/s]

Abbreviations

SFD	Squeeze film damper
ISFD	Integral squeeze film damper
OR-SFD	SFD sealed with O-rings
PR-SFD	SFD sealed with piston rings (PR)

References

[1] San Andrés, L., 2012, *Modern Lubrication Theory*, "Squeeze Film Dampers," Notes 13, Texas A&M University Digital Libraries, http://oaktrust.library.tamu.edu/handle/1969.1/93197 [February 2024].

[2] Vance, J.., 1988, *Rotordynamics of Turbomachinery*, Chapter 3, John Wiley and Sons, New York.

[3] Childs, D.W. 1993, *Turbomachinery Rotordynamics*, Chapter 3, John Wiley and Sons, New York

[4] Zeidan, F., San Andrés, L., and Vance, J., 1996, "Design and Application of Squeeze Film Dampers in Rotating Machinery," Proc. of the 25th Turbomachinery Symposium, Texas A&M University, September, pp. 169-188, https://doi.org/10.21423/R1694R

[5] Della Pietra, L., and Adiletta, G., 2002, "The Squeeze Film Damper over Four Decades of Investigations. Part I: Characteristics and Operating Features, Shock Vib. Dig, (2002), **34**(1), pp. 3-26, "Part II: Rotordynamic Analyses with Rigid and Flexible Rotors", Shock Vib. Dig., (2002), **34**(2), pp. 97-126.

[6] San Andrés, L., Jeung, S-H, Den, S., and Savela, G., 2016 ''Squeeze Film Dampers: A Further Experimental Appraisal of their Dynamic Performance,'' 45th Turbomachinery Symposium, Texas A&M University, Sept 12-15, Houston, TX, https://doi.org/10.21423/R1BC7T

[7] San Andrés, L., and Jeung, S.-H., 2016, "Orbit Model Force Coefficients for Fluid Film Bearings: A Step Beyond Linearization," ASME J. Eng. Gas Turbines Power, **138**(2):022502, https://doi.org/10.1115/1.4031237 (ASME GT2015-43487).

[8] San Andrés, L., and Diaz, S., 2003, "Flow Visualization and Forces from a Squeeze Film Damper with Natural Air Entrainment", ASME J. Tribol., **125**(2), pp. 325-333, https://doi.org/10.1115/1.1510878

[9] Delgado, A., and San Andrés, L., 2010, "A Model for Improved Prediction of Force Coefficients in Grooved Squeeze Film Dampers and Grooved Oil Seal Rings", ASME J. Trib., **132**(3): 032202**.** https://doi.org/10.1115/1.4001459

[10] San Andrés, L., and Koo, B., 2020, "Model and Experimental Verification of the Dynamic Forced Performance of a Tightly Sealed Squeeze Film Damper Supplied with a Bubbly Mixture," ASME J. Eng. Gas Turbines Power, 142(1): 011023, https://doi.org/10.1115/1.4044994 (ASME GT2019-90330).

[11] Koo, B., and San Andrés, L., 2023, "A Model and Experimental Validation for a Piston Rings - Squeeze Film Damper: a Step toward Quantifying Air Ingestion," ASME J. Eng. Gas Turbines Power, 145(4): 0410132, https://doi.org/10.1115/1.4055712 (ASME GT2022-81990).

[12] Gheller, E., Chatterton, S., Vania, A., and Pennacchi, P., 2022, "Squeeze Film Damper Modeling: a Comprehensive Approach," Machines, *10*(9), 781; https://doi.org/10.3390/machines10090781

[13] Lee, G.J., Kim, J., and Steen, T., 2017, Application of Computational Fluid Dynamics Simulation to Squeeze Film Damper Analysis," ASME J. Eng. Gas Turbines Power, **139**(10): 122501. https://doi.org/10.1115/1.4036511

[14] San Andrés, L. and Vance, J., 1987, "Effect of Fluid Inertia on Finite Length Sealed Squeeze Film Dampers," ASLE Transactions, Vol. 30, No. 3, pp. 384-393, https://doi.org/10.1080/05698198708981771

[15] Reinhardt, F., and Lund, J. W., 1975, "The Influence of Fluid Inertia on the Dynamic Properties of Journal Bearings," 1975, ASME J. Lubr. Technol., **97**(1), pp. 154-167.

[16] San Andrés, L., 1985, "Effect of Fluid Inertia Effect on Squeeze Film Damper Force Response," Ph.D. Dissertation, December, Texas A&M University, College Station, TX. https : / /hdl .handle .net /1969 .1 /DISSERTATIONS -428234.

[17] San Andrés, L., 1996, "Theoretical and Experimental Comparisons for Damping Coefficients of a Short Length Open-End Squeeze Film Damper", ASME J. Eng. Gas Turbines Power, 118(4): 810-815, https://doi.org/10.1115/1.2816997.

[18] San Andrés, L., and Delgado, A., 2007, "Identification of Force Coefficients in a Squeeze Film Damper with a Mechanical Seal, Centered Circular Orbit Tests," ASME Journal of Tribology, Vol. 129(3): 660-668, https://doi.org/10.1115/1.2736708 .

[19] Delgado, D., and San Andrés, L., 2010, "Identification of Squeeze Film Damper Force Coefficients from Multiple-Frequency, Non-Circular Journal Motions," ASME J. Eng. Gas Turbines Power, 132(4):042501, https://doi.org/10.1115/1.3159374

[20] Arauz, G., and San Andrés, L., 1997, "Experimental Force Response of a Grooved Squeeze Film Damper, Tribology International, **30**(1)**,** pp. 77-86. https://doi.org/10.1016/0301-679X(96)00033-3

[21] Childs, D.W., Graviss, M., and Rodriguez, L.E., 2007, "The Influence of Groove Size on the Static and Rotordynamic Characteristics of Short, Laminar-Flow Annular Seals", ASME J. Tribol, 129(2), 398-406.

[22] Diaz, S., and San Andrés, L., 1999, "Air Entrainment Versus Lubricant Vaporization in Squeeze Film Dampers: An

Experimental Assessment of their Fundamental Differences," ASME J. Eng. Gas Turbines Power, 123(4): 871-877, https://doi.org/10.1115/1.1383258

[23] Gehannin, J., Arghir, M., and Bonneau, O., 2016, "A Volume of Fluid Method for Air Ingestion in Squeeze Film Dampers," STLE Tribol. Trans., 59(2), pp. 208–218.

[24] San Andrés, L., Koo, B.J., and Seung, J.-H., 2019, "Experimental Force Coefficients for Two Sealed Ends Squeeze Film Dampers (Piston Rings and O-rings): An Assessment of Their Similarities and Differences," ASME J. Eng. Gas Turbines Power, 141(2), 02104, https://doi.org/10.1115/1.4040902 (ASME GT20018-76224).

[25] Jeung, S-H, San Andrés, L., Den, S., and Koo, B., 2019, "Effect of Oil Supply Pressure n the Force Coefficients of a Squeeze Film Damper Sealed with Piston Rings," ASME *J. Tribol*. 141(6): 061701, https://doi.org/10.1115/1.4043238

[26] San Andrés, L., and Rodriguez, B., 2021, "On the Experimental Dynamic Force Performance of a Squeeze Film Damper Supplied through a Check Valve and Sealed With O-Rings," ASME J. Eng. Gas Turbines Power, 143(11): 111011, https://doi.org/10.1115/1.4051964 (ASME GT2021-58627).

[27] Rodriguez, L., and San Andrés, L., 2024, "Dynamic Forced Response of an O-Rings Sealed Squeeze Film Damper Lubricated with a Low Supply Pressure and a Simple Method to Quantify Air Ingestion," ASME J. Eng. Gas Turbines Power, 146(2): 021004, https://doi.org/10.1115/1.4063320 (ASME GT2023-100495).

[28] San Andrés, L., 2012, *Modern Lubrication Theory*, "Experimental Identification of Bearing Force Coefficients," Notes 14, Texas A&M University Digital Libraries, http://oaktrust.library.tamu.edu/handle/1969.1/93197 [February 2024].

[29] Zeidan, F.Y., 1995, "Application of Squeeze Film Dampers," Turbomachinery International, pp. 50-53 (Sept/Oct)

[30] De Santiago, O., and L. San Andrés, 1999, "Imbalance Response and Damping Force Coefficients of a Rotor Supported on End Sealed Integral Squeeze Film Dampers," ASME Paper 99-GT-203, https://doi.org/10.1115/99-GT-203

[31] De Santiago, O., and L. San Andrés, 2003, "Imbalance Response of a Rotor Supported on Flexure Pivot Tilting Pad Journal Bearings in Series with Integral Squeeze Film Dampers," ASME J. Eng. Gas Turb. Pwr, 125(4): 1026-1032, https://doi.org/10.1115/1.1492831.

[32] Delgado, A., Cantanzaro, M., Mitaritonna, N., and Gerbet, M., 2011, "Identification of Force Coefficients in a 5-pad Tilting Pad Bearing with an Integral Squeeze Film Damper," 10th PDF/prime Poitiers Workshop, Poitiers, France, October 6-7.

[33] Agnew, J., and Childs, D., 2012, "Rotordynamic Characteristics of a Flexure Pivot Pad Bearing with an Active and Locked Integral Squeeze Film Damper," ASME Paper GT2012-68564, https://doi.org/10.1115/GT2012-68564

[34] Ertas, B., Delgado, A., and Moore, J., 2018, "Dynamic Characterization of an Integral Squeeze Film Bearing Support Damper for a Supercritical CO_2 Expander," ASME J. Eng. Gas Turb. Pwr., 140(5), p. 052501.

[35] Lu, X., San Andrés, L., Koo, B., and Scott, T., 2021 "On the Effect of the Gap of End Seals on Force Coefficients of a Test Integral Squeeze Film Damper: Experiments and Predictions," ASME J. Eng. Gas Turb. Pwr., 143(1), p. 011014, https://doi.org/10.1115/1.4048700

Acknowledgments

Thanks to the Turbomachinery Research Consortium (TRC) at Texas A&M University for the decades long support. Throughout 30+ years of research, the National Science Foundation, Honeywell Aerospace, Pratt & Whitney Engines, and other private companies funded the work. Dr. San Andrés is indebted to the dozens of graduate students (research assistants) and undergraduate students (student workers) whose work is recognized. The tireless students, eager to learn and passionate of all things engineering, continue to make strides in their respective professional endeavors.

About the author

Luis San Andrés, former Mast-Childs Chair and Professor of Mechanical Engineering at Texas A&M University (1991-2023), conducted experimental and analytical research on the rotordynamics of bearings and dampers for propulsion engines and pump seals and compressor seals for O&G applications. Luis is a Fellow of ASME, STLE, GPPS, and a member of the Industrial Advisory Committees for the Texas A&M Turbomachinery Symposia.

Dr. San Andrés and graduate students published over 200 journal papers, over a dozen papers recognized as best at various international conferences. ASME distinguished Dr. San Andrés with the 2022 Aircraft Engine Technology Award (International Gas Turbine Institute) and the 2023 Mayo D. Hersey Award (Tribology Division). Visit his URL http://rotorlab.tamu.edu for resources on bearings and seals.